The ozone–climate penalty over South America and Africa by 2100

Flossie Brown[1], Gerd A. Folberth[2], Stephen Sitch[3], Susanne Bauer[4,5], Marijn Bauters[6], Pascal Boeckx[6], Alexander W. Cheesman[3,7], Makoto Deushi[8], Inês Dos Santos[6], Corinne Galy-Lacaux[9], James Haywood[1,2], James Keeble[10,11], Lina M. Mercado[2,12], Fiona M. O'Connor[2], Naga Oshima[8], Kostas Tsigaridis[4,5], Hans Verbeeck[6]

[1] College of Engineering, Mathematics and Physical Sciences, University of Exeter, Exeter, UK
[2] College of Life and Environmental Sciences, University of Exeter, Exeter, UK
[3] UK Met Office Hadley Centre, Exeter, UK
[4] Center for Climate Systems Research, Columbia University, New York, NY, USA
[5] NASA Goddard Institute for Space Studies, New York, NY, USA
[6] Department of Environment, Ghent University, Ghent, Belgium
[7] Centre for Tropical Environmental and Sustainability Science, James Cook University, Australia
[8] Meteorological Research Institute, Japan Meteorological Agency, Tsukuba, Ibaraki, Japan
[9] Laboratoire d'Aerologie, Université Toulouse III Paul Sabatier, CNRS, Toulouse, France
[10] Yusuf Hamied Department of Chemistry, University of Cambridge, Cambridge, UK
[11] National Centre for Atmospheric Science (NCAS), University of Cambridge, UK
[12] UK Centre for Ecology and Hydrology, Wallingford, UK

Correspondence to: Flossie Brown (fb428@exeter.ac.uk)

Abstract

Climate change has the potential to increase surface ozone (O_3) concentrations, known as the 'ozone–climate penalty', through changes to atmospheric chemistry, transport and dry deposition. In the tropics, the response of surface O_3 to changing climate is relatively understudied, but has important consequences for air pollution, human and ecosystem health. In this study, we evaluate the change in surface O_3 due to climate change over South America and Africa using 3 state-of-the-art Earth system models that follow the Shared Socioeconomic Pathway 3 7.0 emissions scenario from CMIP6. To quantify the changes driven by climate change alone, we evaluate the difference between end of the century predictions for simulations which include climate change and simulations with the same emissions scenario but with a fixed present-day climate. We find that by 2100, models predict an ozone–climate penalty in areas where O_3 is already predicted to be high due to the impacts of precursor emissions, namely urban and biomass burning areas, although on average models predict a decrease in surface O_3 due to climate change. We identify a small but robust positive trend in annual mean surface O_3 over polluted areas. Additionally, during biomass burning seasons, seasonal mean O_3 concentrations increase by 15 ppb (model range 12 to 18 ppb) in areas with substantial biomass burning such as the arc of deforestation in the Amazon. The ozone–climate penalty in polluted areas is shown to be driven by an increased rate of O_3 chemical production, which is strongly influenced by NOx concentrations and is therefore specific to the emissions pathway chosen. Multiple linear regression finds the change in NOx concentration to be

a strong predictor of the change in O_3 production whereas increased isoprene emission rate is positively correlated with increased O_3 destruction, suggesting NOx-limited conditions over the majority of tropical Africa and South America. However, models disagree on the role of climate change in remote, low-NOx regions, partly because of significant differences in NOx concentrations produced by each model. We also find that the magnitude and location of the ozone–climate penalty in the

40 Congo basin has greater inter-model variation than in the Amazon, so further model development and validation is needed to constrain the response in central Africa. We conclude that if the climate were to change according to the emissions scenario used here, models predict that forested areas in biomass burning locations and urban populations will be at increasing risk of high O_3 exposure.

1. Introduction

45

Climate change threatens to bring new pressures to the tropical forests, grasslands and agricultural lands of Africa and South America. As a result of shifts in emissions, atmospheric chemistry, and meteorology, as well as changes in vegetation behaviour such as transpiration rate, surface O_3 concentrations are likely to change (e.g. Turnock et al., 2019; Griffiths et al., 2021; Zanis et al., 2022), which may impair or benefit human and vegetation health (Agathokleous et al., 2019; Emberson,

50 2020) depending on the direction of change. O_3 is a highly oxidising compound, formed in the atmosphere through reaction of volatile organic compounds (VOC) with hydroxyl radicals (OH), and, during the night-time, nitrate radicals (NO_3) in the presence of nitrogen oxides (NOx). However, it can also be removed from the atmosphere through reactions with many of the same chemical species (NOx, VOC, OH) depending on their relative concentrations. In addition to chemical pathways, O_3 can be removed from the lower atmosphere by dry deposition, which includes stomatal uptake by plants (Silva & Heald, 2018).

55 Stomatal uptake of O_3 and subsequent ozone–plant damage, can lead to reduced carbon drawdown from the atmosphere (Sitch et al., 2007; Yue & Unger, 2018; Franz & Zaehle, 2020), and changes to biosphere–climate interactions (Sadiq et al., 2017). Sitch et al. (2007) showed that the tropics may be especially sensitive to high O_3 concentrations and therefore susceptible to large productivity losses if surface O_3 were to increase. Additionally, O_3 is a near-term climate forcer with impacts on the radiative balance leading to a positive radiative forcing of climate through increases in anthropogenic precursors (Oswald et

60 al., 2015; Coates et al., 2016; Romer et al., 2018). As the tropical forests are vital as sinks for atmospheric CO_2, and tropical ecosystems play a vital role in regional and global climate (Lewis, 2006; Bonan, 2008), an understanding of the impact of climate change on surface O_3 concentrations in the tropics is critical.

Whilst there have been no studies specifically assessing changes in surface O_3 due to climate change in the tropics, global

65 studies have suggested that changes in temperature-dependent chemistry, natural emissions of precursors, transport and land surface properties may lead to an 'ozone–climate penalty over some continental areas (Jacob & Winner, 2009; Doherty et al., 2013; Zanis et al., 2022). The 'ozone–climate penalty' is defined as an increase in surface O_3 concentrations due to climate

change alone. It is influenced by many complex chemical and biological processes, which are not all well-understood or represented in current climate models, although there has been substantial recent research to reduce uncertainty in temperature-sensitive chemistry, meteorology and land–atmosphere feedbacks (Oswald et al., 2015; Coates et al., 2016; Sadiq et al., 2017; Romer et al., 2018; Archibald et al., 2020b). There has been relatively little research focusing on O_3 in tropical environments. Unlike the more commonly studied extra-tropical Northern hemisphere, the tropics have relatively low (natural) NOx emissions and high biogenic VOC emissions, high actinic flux and strong atmospheric convection (Bond et al., 2002; Pugh et al., 2010; Paulot et al., 2012). This paper focuses on South America and Africa. We exclude equatorial Asia because the atmospheric chemistry in this region is more uncertain due to difficulties in detecting and accounting for peat fire emissions (Prosperi et al., 2020). Equatorial Asia has a greater marine influence and most model grid boxes contain ocean as well as land, so it may also follow a different chemical regime.

Many areas in Africa and South America are considered remote (defined in this paper by low emissions of NOx), although increasing anthropogenic activity such as urbanisation and biomass burning causes moderate NOx emissions in some regions (e.g. Kuhn et al., 2010; Pacifico et al., 2015; Shi et al., 2020). The sensitivity of O_3 production to NOx depends on the relative concentrations of NOx and VOCs. Biogenic isoprene is the major O_3-forming non-methane VOC and must be oxidised in the atmosphere before it can form O_3 (Liu et al., 2016). NOx is produced from both natural and anthropogenic sources including lightning, transport and biomass burning. In severely NOx-limited regions, increasing isoprene acts to reduce O_3 concentrations through oxidation and formation of isoprene nitrates (Pacifico et al., 2012). In this NOx-limited case, increasing NOx will lead to greater O_3 formation. Conversely, in highly polluted areas with sufficient NOx present, increasing NOx concentrations may inhibit O_3 formation by direct reaction and removal of $O3$ with NOx.

Earlier studies have found that South America and Africa are NOx-limited (Ziemke et al., 2009; Bela et al., 2015), and that increases in NOx concentration associated with climate change will be a key driver of O_3 increases over South America and Africa. Doherty et al. (2013) attribute the NOx increase predominantly to enhanced decomposition of the NOx reservoir species, peroxyacetyl nitrate (PAN). A fraction of emitted NOx is locked up as PAN, which decomposes back into NOx in warmer temperatures, sometimes after having travelled long distances from the NOx source. As PAN is unstable at high temperatures, climate change will result in a smaller fraction of NOx being stored as PAN in NOx source regions and may also decrease the amount of NOx that is transported into remote regions (Schultz et al., 1999; Finney et al., 2018). Lightning NOx is known to contribute to O_3 formation, however studies project both increases and decreases in future lightning frequency (Clark et al., 2017; Finney et al., 2018) leading to low confidence in how O_3 will be affected by climate-driven changes in lightning (Fu & Tian, 2019; Murray, 2016).

The role of isoprene in the ozone–climate penalty is debated as there is uncertainty about how isoprene emissions will change in the future in response to temperature, CO_2 and land-use change (Fu & Liao, 2016; Fu & Tian, 2019) and how to best

represent isoprene chemistry in climate models (Weber et al., 2021). Biogenic isoprene emissions increase strongly with temperature and vegetation stress (e.g. Guenther et al., 1993; Niinemets et al., 1999; Unger et al., 2013; Morfopoulos et al., 2021), but very high temperatures or moisture stress may cause 'die-back' of vegetated areas, which would decrease isoprene
105 emissions overall (Sanderson et al., 2003; Cox et al., 2004; Malhi et al., 2009). On the other hand, elevated CO_2 concentrations directly inhibit isoprene emission but can indirectly increase emission if this CO_2 fertilisation effect results in increased plant productivity (Pacifico et al., 2011; Squire et al., 2014; Hantson et al., 2017).

Besides chemical processes, dry deposition of O_3 to vegetation is a major O_3 sink, accounting for 20% of O_3 removal (Wedow
110 et al., 2021). Most O_3 deposition occurs via plant stomata, which respond to changes in the climate. (Silva & Heald, 2018; Clifton et al., 2020). Increased CO_2, temperature and vapour pressure deficit (VPD) will decrease stomatal conductance and therefore decrease O_3 deposition rate. This could lead to increased concentrations of O_3 in the atmosphere, although it would have a protective effect for plants (Emberson et al., 2013; Lin et al., 2020).

115 Studies agree that over the ocean, average surface O_3 concentrations will decrease under the influence of climate change due to increased formation of OH (Zeng et al., 2008; Doherty et al., 2013; Zanis et al., 2022). OH increases because the warmer air can hold more water vapour, leading to increased destruction of O_3. There may also be O_3 reductions in remote regions over land due to this process although natural emissions can change the atmospheric chemistry over the continents. Other factors contributing to the O_3 concentration over the continents are numerous and complex, including changes to oxidising
120 capacity, stratospheric transport and land-use (Archibald et al., 2010; Squire et al., 2015).

This paper quantifies the effect of climate change on surface O_3 concentrations in the future, with aims to understand its uncertainty and the relative contributions of the underlying processes. We focus on areas with robust O_3 changes in O_3 to identify areas in South America and Africa at greatest risk by 2100. Section 1 has introduced the key chemical species involved
125 in O_3 chemistry and the most important changes that may result from climate change. In Section 2, we provide the model details, data used for evaluation, and description of analysis of model output. Section 3 evaluates model predictions of surface O_3 in the present-day, evaluates model predictions for surface O_3 changes in 2100 and examines the importance of chemical and deposition changes in controlling the ozone–climate penalty in models. Finally, Section 4 discusses the key trends predicted by the models, limitations of the study and crucial uncertainties in the models.

130

2. Methods

We analyse surface O_3 for simulations that follow a medium-high emissions pathway created for CMIP6 (Pascoe et al., 2019). The simulations were carried out as part of an ensemble of Earth system model experiments designed to quantify the climate

and air quality impacts of aerosols and trace gases in climate models (Collins et al., 2017) named Aerosol-Chemistry Model
135   Intercomparison Project (AerChemMIP). For this study three Earth system models were used: UKESM1-0-LL (abbr.
UKESM1), GISS-E2-1-G (abbr. GISS), MRI-ESM2-0 (abbr. MRI). These were selected because of their detailed tropospheric
chemistry schemes and availability of output for O_3 and O_3 precursor concentrations on the Earth System Grid Federation
(ESGF).

140   The simulations follow the Shared Socioeconomic Pathway 3 7.0 (SSP3-7.0) emissions scenario, a scenario assuming low
international cooperation to protect the environment. This includes high emissions of non-methane near-term climate forcers
and substantial land-use change (O'Neill et al., 2016; Gidden et al., 2019). The prescribed emissions include anthropogenic
and biomass burning emissions of NO, CO_2 and CO (Rao et al. 2017; Riahi et al., 2017) and the future pathway for CH_4 is
calculated as an atmospheric concentration (Meinshausen et al., 2019). Emissions due to growing populations and poor
145   international cooperation results in significant temperature increases by 2100 (Turnock et al., 2019) and societies that are
highly vulnerable to climate change. This emissions pathway was chosen in order to understand changes in end-of-century O_3
concentration if there is no international cooperation to reduce precursor emissions.

2.1 Model descriptions

Here we provide a brief description of the Earth system models and their tropospheric chemistry schemes that are relevant to
150   this study.

UKESM1-0-LL (abbr. UKESM1)

UKESM1-0-LL is a combination of HadGEM3 (Williams et al., 2018) with additional land and atmospheric chemistry
components (Sellar et al., 2019). The UK Chemistry and Aerosol scheme (UKCA) contains stratospheric and tropospheric
155   chemistry (Archibald et al., 2020a) combined with the GLOMAP-mode aerosol microphysics scheme (Mulcahy et al., 2018,
Mulcahy at al., 2020).

Interactive emissions include isoprene, monoterpenes,lightning NOx and soil NOx. Isoprene and monoterpene emissions
respond to light and temperature and the isoprene scheme also includes CO_2 inhibition (Archibald et al., 2020a; Mulcahy et
160   al., 2018) following the emission model of Pacifico et al. (2011). Lightning NOx is calculated using the parameterisation of
Price and Rind (1992). SOA is calculated as a fixed yield of 26% from gas-phase oxidation reactions involving monoterpene
sources.

The terrestrial biogeochemistry is provided by JULES (Wiltshire et al., 2019; Wiltshire et al., 2021). Stomatal conductance in
165 JULES is similar to the Ball-Berry-Leuning model (Leuning, 1995) and responds to the ratio of internal to external CO_2
concentrations and leaf humidity deficit (Jacobs, 1994).

The model has a horizontal resolution of 1.25° latitude by 1.875° longitude with 85 vertical levels in a hybrid height coordinate.

170 **MRI-ESM2-0 (abbr. MRI)**

MRI-ESM2-0 (Yukimoto et al., 2019; Kawai et al., 2019; Oshima et al., 2020) contains an atmospheric and land-surface model
(MRI-AGCM3.5), an ocean and sea-ice model (MRI.COMv4), an aerosol model (MASINGAR mk-2r4c) and an atmospheric
chemistry model (MRI-CCM2.1). The chemistry model includes tropospheric, stratospheric and mesospheric chemistry with
175 90 chemical species and 259 chemical reactions (Deushi & Shibata, 2011).

Lightning NOx is interactive (Price & Rind, 1992) but natural emissions from land and ocean are prescribed as monthly
climatologies, including isoprene and soil NOx (Deushi & Shibata, 2011). 15% of natural terpene emissions at the surface
form SOA and SOA have identical properties to POA.
180
Each component employs different horizontal resolutions but the outputs used in this paper are from the chemistry component
which uses a horizontal resolution of 2.8125° latitude by 2.8125° longitude with 80 vertical levels in a hybrid sigma pressure
coordinate.

185 **GISS-E2-1-G (abbr. GISS)**

GISS-E2-1-G contains a coupled troposphere and stratosphere chemistry scheme using the G-PUCCINI chemistry mechanism
(Shindell et al., 2013; Kelley et al., 2020) combined with the One-Moment Aerosol (OMA) scheme for aerosols (Bauer et al.,
2020).
190
Lightning NOx is interactive as described by Kelley et al. (2020). Natural emissions include soil NOx and isoprene, which
respond to light and temperature (Shindell et al., 2006) following the algorithm defined by Guenther et al., (1995).
Monoterpenes are prescribed. SOA is calculated using the CBM4 chemical mechanism to describe the gas phase tropospheric

chemistry together with all main aerosol components including SOA formation and nitrate, and is calculated using four tracers
195 in the model. Isoprene (VOCs) contribute to the formation of SOA (Tsigaridis et al., 2018).

GISS has a horizontal resolution of 2.00° latitude by 2.25° longitude with 40 vertical levels output on hybrid sigma pressure
coordinate.

200 **2.2 Data analysis methods**

Model evaluation

In situ observations from 65 sites across South America and tropical Africa, covering key biomes and land-use types, are used
for grid level model evaluation. Monthly mean O_3 concentrations from individual sites have been aggregated into 7 regions by
grouping together sites within latitude and longitude bounds (see Table S1). To compare to models, the coordinates of the in
205 situ measurement sites are matched to the nearest model grid cell coordinates. To create an average seasonal cycle for each
region, sites with the same nearest grid cell are averaged together to create a grid cell seasonal cycle. Then, grid cell seasonal
cycles in the same region are averaged together. Monthly mean data from 1990 up to the 2021 were used, although most sites
only provide a few years of data. Data were excluded if there was an unequal distribution of data points over the monthly mean
diel cycle.
210

For the model seasonal cycle, the monthly mean O_3 concentration in all grid cells containing observation sites was calculated
using CMIP6 historical simulations for the period 1990–2014. The standard deviation in monthly mean O_3 concentrations
between the grid cells used was calculated for each region (i.e. it represents variation in O_3 geographically between the sites
rather than inter-annual variation).
215

For model evaluation against Tropospheric Emission Spectrometer (TES) data from the Aura satellite, which retrieves O_3 in
ppb over 67 pressure levels, we use O3 concentrations at the lowest level available from TES (825 hPa). Monthly mean gridded
outputs are used for the period 2004–2011, the period for which complete monthly mean data is available. As with the model
output, satellite grid cell coordinates closest to the in situ site coordinates were selected. The monthly mean and standard
220 deviation for each region was calculated, only using data from grid cells containing in situ sites.

CMIP6 model output

We isolate the effect of climate change on surface O_3 concentrations using the difference between two simulations which
consider the same trajectory of anthropogenic emissions changes but differ in climate. The simulations are fully-coupled,
global model runs driven with prescribed sea surface temperatures (SSTs) over the period 2015–2100. We use a simulation

225 driven with changing SSTs from the coupled simulation ssp370 so that the climate changes in accordance with the emissions changes, this simulation is named ssp370SST. We use a second simulation with prescribed SSTs are sea ice concentrations taken from a present-day climatology (2005–2014) in historical simulations, named ssp370pdSST. Importantly, although emissions are identical in both simulations, ssp370pdSST does not include the resulting climate change. To isolate the effect of climate change on tropospheric O_3, we subtract ssp370pdSST (present-day constant climate + future emissions) from

230 ssp370SST (future climate + future emissions) following Zanis et al. (2022). Biomass burning and land-use change are considered anthropogenic and are prescribed for both models but natural emissions are allowed to change depending on the model set-up. In this way, the background atmospheric composition is based on the future emissions scenario used, since the response of atmospheric chemistry to climate change may depend on the background concentrations of precursors. In UKESM1, CO_2 is also fixed to present-day concentrations in ssp370pdSST to avoid inhibiting isoprene emission by CO_2.

235

Model output is taken as monthly means during the period 2090–2100 between 40°S and 40°N from experiments ssp370SST and ssp370pdSST. All variables used are outlined in Table S2. The change due to climate change refers to subtracting ssp370pdSST from ssp370SST, where positive values are considered an O3–climate penalty. When evaluating the change due to climate change regionally, this study distinguishes between 'high-NOx' and 'remote' areas (Fig. 1). High-NOx areas are

240 defined as areas where the annual mean NOx emissions are above the 95th percentile for the entire tropics (40°S–40°N).

O3 concentrations are taken from the lowest model level (~ 20 m above canopy). Where multi-model means are shown, data has been re-gridded to the 2.8125° by 2.8125° grid used by MRI. We evaluate the ozone–climate penalty as a yearly average and seasonally. To identify seasonal patterns we aggregate the data by burning season. The Western African burning season is

245 defined as Dec–Feb, the Southern African burning season is June and July and the Southern Amazon burning season is Aug–Oct.

To attribute the ozone–climate penalty to precursor variables, we also use NOx, isoprene emission rate, OH and surface temperature variables. When presenting these variables, the ocean has been masked so that only land surface changes are

250 presented. 'Surface concentrations' shown in this study refer to chemical mixing ratios in the lowest model grid cells and 'background concentrations' refer to chemical mixing ratios in the absence of climate change (using data from ssp370pdSST).

To evaluate the O_3 budget, we also use O_3 chemical production, O_3 chemical loss and dry deposition variables. To compare these three variables on the same scale, we convert the units to Tg year[-1] and sum production and loss over the lowest 1 km,

255 the approximate boundary layer height. We choose 1 km to establish an approximate region that can contribute to surface O_3 concentrations.

In Sect. 3.4, we present a sensitivity study relating changes in NOx concentration and isoprene emissions (see isoprene representation in this paper S2) to changes in O_3 chemical production. We use monthly mean data in South America and Africa

260 within 40°S and 40°N to calculate a monthly climatology for 2090–2100, masking the ocean. To identify the limiting O_3 precursor in the tropics, the percentage change in O_3 production rate ($n>500$) is modelled with an ordinary least squares linear regression using the percentage change in NOx and isoprene as predictor variables (see the relationship between NOx and O_3 production S4). To interpret the ability of the model we rely on the central limit theorem to assume that the normalised sum of the residuals can be approximated by a normal distribution. Unique months and grid cells are treated as separate data points.

265 To present the results graphically, we highlight values using star markers if they are above a threshold of the 95th percentile for NOx concentrations using the monthly climatology for each model individually, with aims to identify biomass burning areas and cities. The atmospheric chemistry in these areas may be different due to the elevated NOx concentrations. Therefore, some grid cells will be above the 95th percentile for specific months only (biomass burning seasons).

3. Results

270 ### 3.1. Evaluation of model skill for present-day surface O_3 concentrations

Results show the climate models are able to capture the observed seasonal cycle in most regions except for West Africa and DR Congo (Fig. 1). However, the models overpredict monthly mean surface O_3 concentrations by up to 50 ppb, with the largest bias present in remote forest locations such as the Congo area (Fig. 1e). GISS overall has the smallest positive bias out of all the models, and MRI has the largest. UKESM1 shows the smallest seasonal variation in O_3 concentration, which is often closer

275 to the observed seasonal pattern.
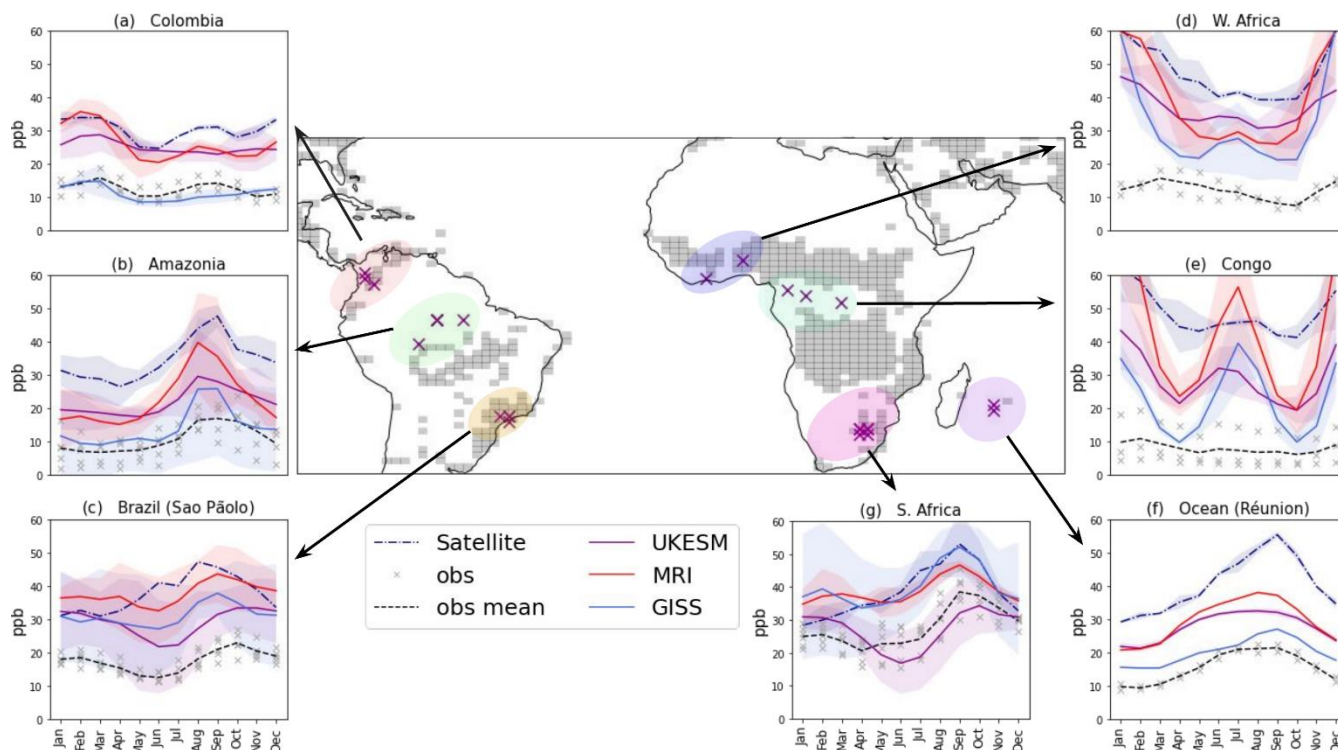
Figure 1: panels a–g compare monthly mean O3 (black dashed line) from site measurements averaged over 7 regions to model predictions for the period 2015–2020 and satellite products from the TES satellite at 825 hPa (navy dash-dot line). Model means are shown for UKESM1 (purple solid line), GISS (blue solid line) and MRI (red solid line) and 2 standard deviations from the mean are shaded. Grey crosses indicate monthly mean O3 measurements from individual sites and years.

The central panel marks the locations where O3 measurement sites are located (purple crosses) and how the sites have been grouped (coloured shading). Observations 1a–1c and 1f–1g use data from the Tropospheric O3 Assessment Report (TOAR I, Schröder, 2021; Schultz et al., 2017), 1d and 1e from INDAAF (http://www.indaaf.obs-mip.fr) and 1e from CONGOFLUX in Yangambi, DR Congo. Grey grid cells cover areas where NOx emissions are above the 95th percentile for the tropics in 2100 (prescribed by (Rao et al., 2017; Riahi et al., 2017), indicative of biomass burning areas and cities. Un-shaded areas are referred to as 'remote' throughout.

Grey shading on Fig. 1 highlights the areas in South America and Africa with the highest NOx emissions. The shaded areas represent areas with high biomass burning emissions and urban areas and are referred to as 'high-NOx' areas in this paper. In the Southern Amazon (Fig. 1b), the biomass burning months are August and September and both models and observations predict the highest O3 concentrations in this season. However, the observed monthly mean O3 concentrations fall within 9 to 20 ppb whereas models predict values up to 40 ppb, with GISS displaying the smallest positive bias. In Africa (Figs 1d–1f), the biomass burning months are December–February (North / West Africa) moving to June–July (Southern Africa). Whilst models predict concentrations of up to 80 ppb in the Congo during these months due to transport of precursors from biomass burning, observations show substantially lower surface O3 concentrations of less than 20 ppb at the remote locations sampled, although the highest O3 concentrations occur during December–February (Adon et al., 2010; 2013; Ossohou et al., 2019). In

fact, seasonal variation is low at the Congo sites whereas models predict strong seasonal patterns (Fig. 1e). In months without substantial burning, GISS captures the low O_3 values well and UKESM1 and MRI overestimate by 10 to 15 ppb.

300   The enhanced O_3 concentrations predicted by models in burning seasons over the Congo and West Africa are also captured in satellite retrievals at 825 hPa. Satellite O_3 concentrations in the DR Congo are 10 ppb higher in Dec–Feb compared to months without burning (Fig. 1e). At 825 hPa, these satellite capture O_3 concentrations above the altitude of in situ observation sites and the lowest model level. Model predictions for O_3 at 825 hPa are ~10 ppb higher than the lowest model level and therefore compare well to satellite retrievals (Fig. S1), especially in Amazonia (Fig. S1b) and West Africa (Fig. S1d).

305

Similar to biases over the remote continents, measurements from Réunion Island (Fig. 1f), which capture oceanic air masses, are overestimated by 5 ppb in GISS and by 12 ppb in UKESM1 and MRI, although the seasonal cycle is reproduced. On the other hand, over the urban sites in South Africa, Johannesburg, UKESM1 replicates the observed mean with moderate accuracy, whereas GISS and MRI overestimate by 15 ppb (Fig. 1g).

310   **3.2. Average changes to atmospheric composition over Africa and South America at the end of 2100**

The overall change in O_3 concentration due to climate change over the African and South American land surface is shown in Fig. 2a for each model compared to the simulation with a fixed present-day climate. All models predict that on average O_3 concentrations will decrease due to climate change over the tropical land surface in this study. The magnitude of the predicted O_3 change for each model will depend on background concentrations of O_3 chemical precursors, their change due to climate change and individual model mechanistic details. There is significant diversity in background atmospheric composition

315   between models (Fig. 2, blue marker) and the direction of change in surface NOx and OH concentration due to climate change varies (Figs 2b, 2c, arrows).

Different temperature sensitivities of the models (differing by up to 2.7 K) and different biogenic VOC schemes will contribute

320   to the inter-model variation (Fig. S2). UKESM1 has the greatest temperature sensitivity with a 6.5 K increase in temperature over the tropical land surface due to climate change (Fig. 2e). The temperature change due to climate change varies seasonally and regionally, which may affect concentration of ozone precursors locally (discussed further in Sect. 3.4), with dry seasons temperatures predicted to rise by 1–1.5 K more than wet season temperatures (Fig. S3).
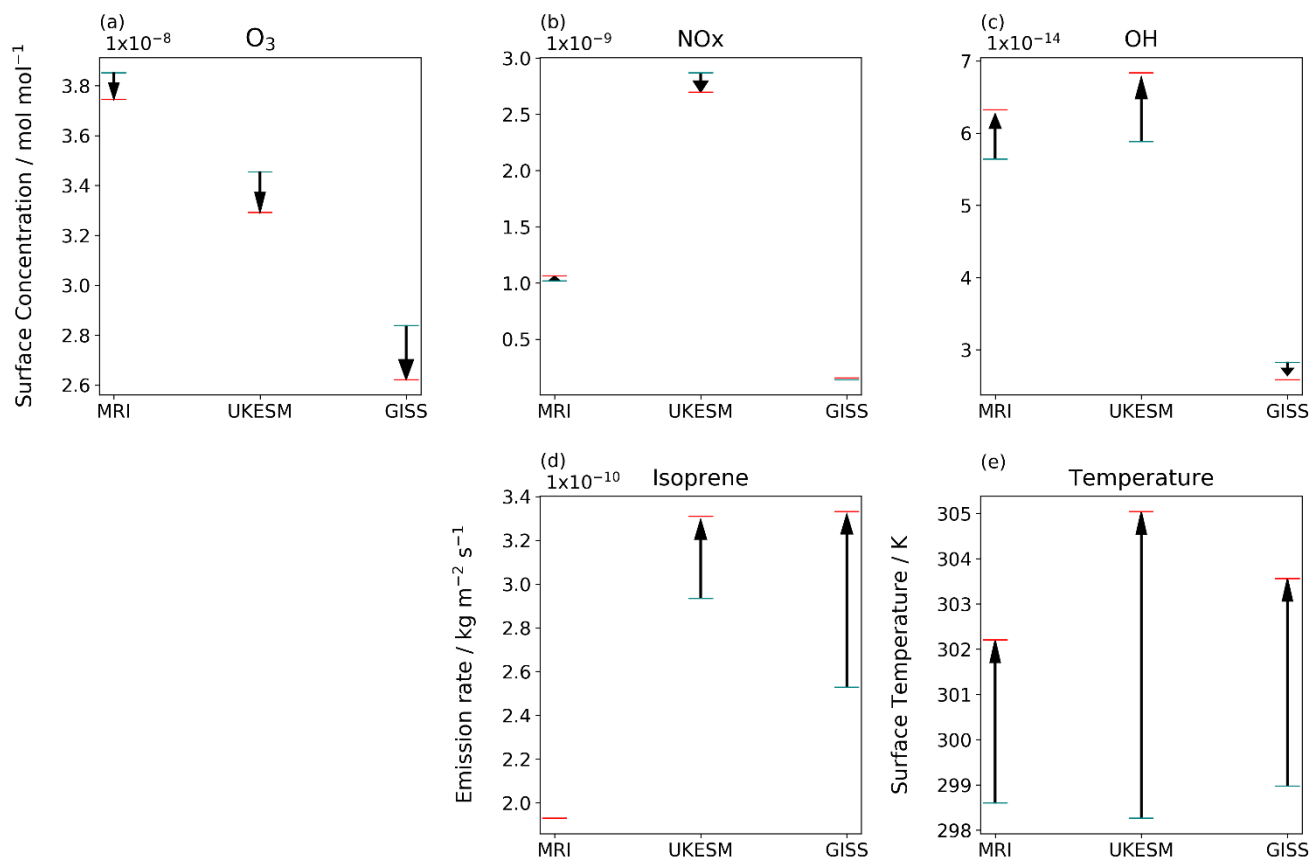
Figure 2: The change in surface concentration of (a) O3 (b) NOx , (c) OH, and the change in (d) isoprene emission rate and (e) surface temperature and from experiment ssp370pdSST with no climate change (blue line) to experiment ssp370SST with climate change (red line) for the three climate models in this study. Variables have been averaged over the African and South American continents between 12° N–30° S for the period 2090–2100. The change due to climate change is significant at the 5% level for all variables and models except isoprene in MRI (which is prescribed so does not change).

NOx emissions, including biomass burning emissions, are prescribed based on the SSP3-7.0 scenario but lightning NOx differs between the models based on the chosen parameterisation of individual models. Compared to the present-day, NOx emissions in biomass burning areas decrease in Africa to follow projected trends, but do not change in South America. NOx emissions increase in cities and Nigeria especially has major growth in urban areas. Additionally, lightning NOx emissions can change due to climate change. In all models, lightning NOx emissions increase due to climate change and the locations of the increases vary in latitude to follow the wet season (not shown).

The increase in isoprene emission rate due to climate change depends on the isoprene emission scheme used, or in MRI, isoprene emissions are prescribed as a climatology. The greatest increase in isoprene emissions rate occurs in the GISS model,

340   which increases from 2.5 x10^{-10} kg m^{-2} s^{-1} to 3.3 x10^{-10} kg m^{-2} s^{-1} when climate change is considered, whereas UKESM1, which accounts for CO_2 inhibition, increases more modestly from 2.9 kg m^{-2} s^{-1} to 3.3 x10^{-10} kg m^{-2} s^{-1}. Isoprene emissions are presented throughout rather than isoprene concentrations (see Isoprene representation in this paper S2).

3.3 Changes in surface O3 concentration due to climate change over remote regions compared to high-NOx areas

This study focuses on the change in surface O_3 concentration over land in 2100, although we note there are significant decreases
345   in O_3 concentration over the oceans and non-vegetated areas such as Saharan Africa (Fig. 3). Over land, the multi-model mean shows increases of up to 4 ppb over urban areas and the biomass burning areas of South America and Africa (Fig. 3a) whereas ocean-influenced locations such as Northeast Brazil are expected to benefit by a 4 to 5 ppb decrease in surface O_3. However, the direction of change in surface O_3 concentration over central Africa and the remote Amazon (North West) is not robust between models (Fig. 3c, 3d, 3e).

350
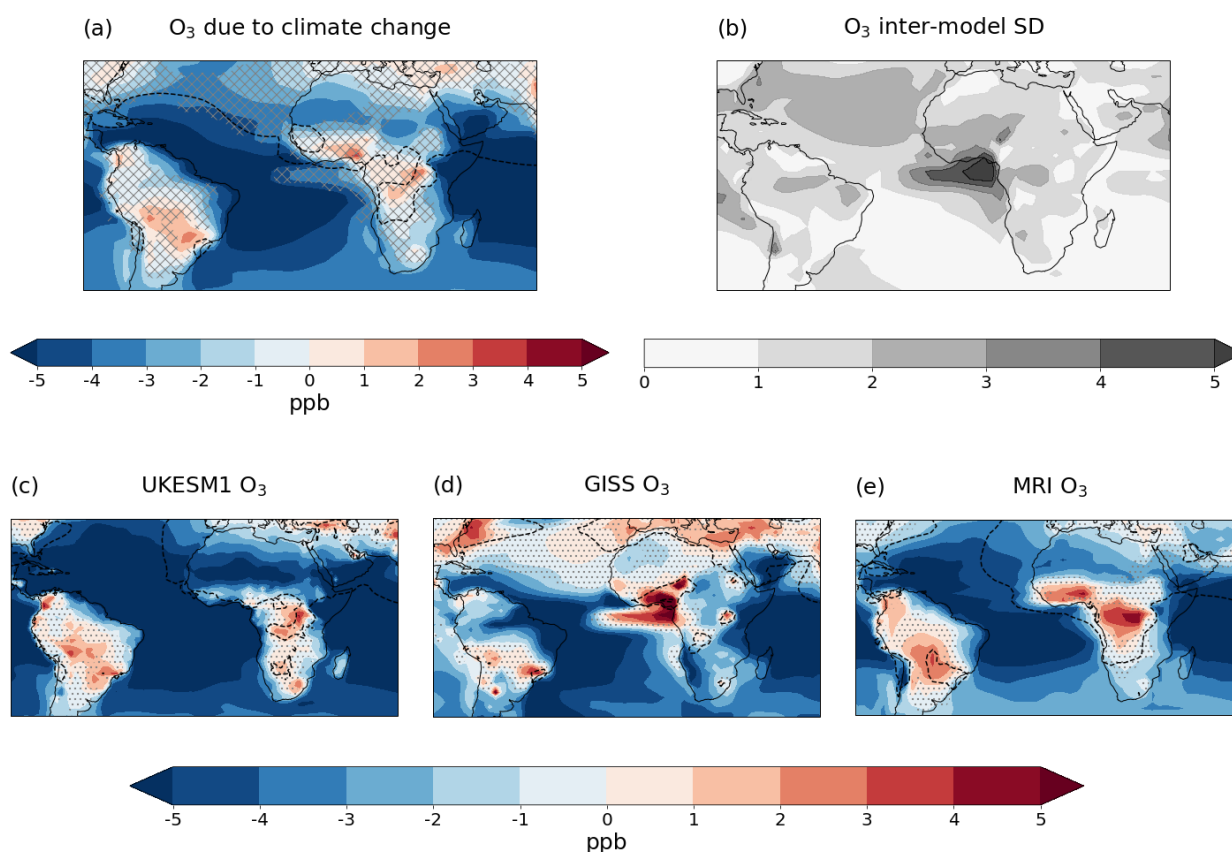
Figure 3: The average change in surface O3 concentration due to climate change for the period 2090–2100 for (a) the multimodel mean, (c) UKESM1 only, (d) GISS only, (e) MRI only. (b) shows the inter-model standard deviation in the same units. Grey hatching in (a) covers areas where the inter-model standard deviation is greater than 20% of the multimodel mean value. Grey dots in panels (c)–(e) cover areas that are not significant at the 5% level from a student's t-test. Black dotted lines outline areas where background
355   O3 is higher than 40 ppb.

UKESM1 and MRI predict increases in surface O_3 concentration of up to 5 ppb in the Amazon and central Africa, with decreases over coastal regions due to climate change (Figs 3c, 3e). In the remote Amazon, MRI predicts an increase and UKESM1 a decrease in O_3 concentration, but neither change is significant. On the other hand, GISS predicts significant O_3

360   decreases across remote regions of up to 4 ppb (Fig. 3d), including central Africa which experiences O_3 increases in the other simulations (Figs 3c, 3e).

Changes in surface O_3 concentration due to climate change in 2100 are shown in Fig. 4, grouped by regional biomass burning season, with dotted contours where background O_3 is 40 ppb (a number assumed associated with thresholds for plant O_3

365   damage) and 70 ppb. High background O_3 is associated with biomass burning and pollution in and around cities due to their higher NOx emissions. These high O_3 areas also show the greatest increase in O_3 due to climate change (Fig. 4).
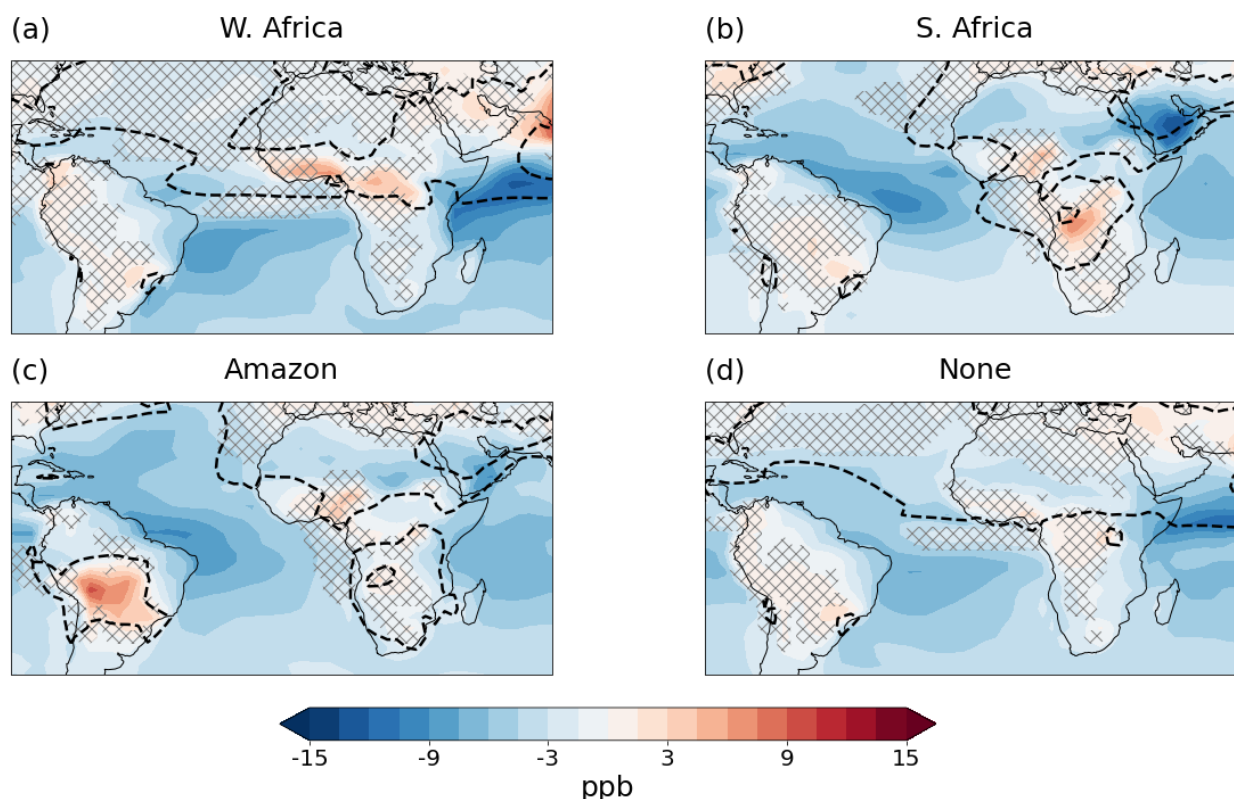
Figure 4: The multimodel mean change in surface O3 concentration for the period 2090–2100 for (a) the Western African burning season (Dec–Feb), (b) the Southern African burning season (June, July), (c) the Southern Amazon burning season (Aug–Oct), and
370   **(d) the remaining months with limited burning (March–May, Nov). Grey hatching covers areas where models disagree on the sign of the change due to climate change. Black dotted lines outline areas where background O3 is higher than 40 ppb and 70 ppb.**

During December–February, the biomass burning area in Western Africa coincides with O_3 increases of 9 ppb (5 ppb for UKESM1, 7 ppb for MRI and 15 ppb for GISS, Fig. 4a) and similar penalties are seen for Southern African biomass burning

375 periods during June–August (Fig. 4b). During the Amazon biomass burning season, there are even larger increases of up to 12 ppb in the Southern Amazon (Fig. 4d). In months without biomass burning, these areas have minor increases of 2 ppb for UKESM1 and MRI and a decrease of 3 ppb for GISS (Fig. 4c).

GISS is the only model to show significant decreases in monthly mean surface O_3 concentration over land, which consistently

380 occur in areas and seasons with low background O_3 (not shown). This includes biomass burning areas but in seasons without burning (Fig. 4d), which are followed by large increases in the biomass burning season. The result is that seasonal changes in surface O3 concentration due to climate change in GISS are much more extreme than UKESM1 and MRI and models do not agree on the direction of change in remote areas, although the yearly average increase is similar between models (Fig. 3). This results in uncertainty in the response to climate change from regions and seasons with low background O_3, but likely increases

385 in areas and seasons with high background O_3 from anthropogenic NOx emissions (Fig. 4, black dashed lines).

Emissions from cities create consistent increases in O_3 concentration in all months, leading to an increase of up to 5 ppb in the yearly average. In particular, megacities in Nigeria (Lagos), Brazil (São Paulo, Rio de Janeiro) and Colombia (Bogotá, Medellín) can be identified by a 3 ppb increase in all seasons, which is robust over Southeast Brazil (Fig. 4).

390 **3.4 Changes in chemical production and deposition of O_3 due to climate change**

Attribution of changes in surface O_3 to changes in chemical production, chemical loss and dry deposition at the surface are shown in Fig. 5. The increase in O_3 production due to climate change is the largest out of these terms (Fig. 5c) and increases the most (over 0.25 Tg year^{-1}) in high-NOx areas where surface O_3 increases (Fig. 5a). Therefore, the increase in the rate of

395 O_3 production is likely to be the main cause of the ozone–climate penalty in high-NOx areas (high-NOx defined as in Fig. 1). Removal of O_3 by deposition and chemical destruction has a smaller effect on O_3 concentration since, to a degree, the two terms cancel each other out; in high-NOx areas, chemical loss increases by up to 0.1 Tg year^{-1} and dry deposition decreases by up to 0.05 Tg year^{-1}. In remote regions, there is considerable variation between models as indicated by the higher standard deviation in these areas (Figs 5, column 2). GISS predicts decreases in O_3 production over remote regions of up to 0.1 Tg year^{-1}

400 ^{1} and increases of up to 0.25 Tg year^{-1} over high-NOx regions, whereas MRI and UKESM1 predict increases in O_3 production across all regions except Saharan Africa. MRI predicts the largest increases in O_3 chemical production in remote areas of 0.25 Tg year^{-1} (not shown).
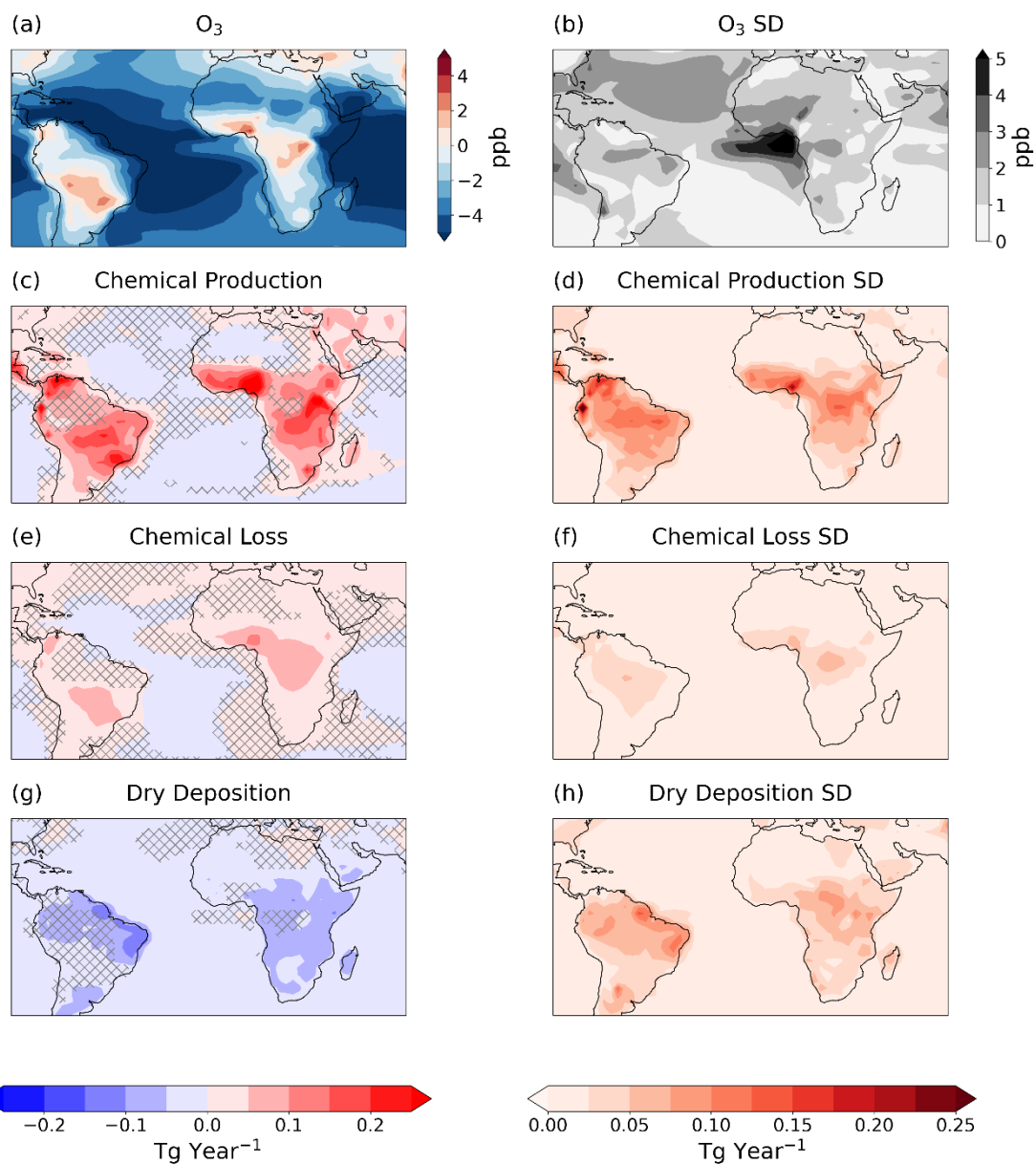
Figure 5. The multi-model mean change in (a) surface O3 concentration, (c) chemical production of O3, (e) chemical destruction of O3 and (g) dry deposition of O3 due to climate change. Panels (c), (e) and (g) show the change in O3 in Tg year[-1] and chemical terms have been summed over a 1 km height. The inter-model standard deviations are shown in panels (b), (d), (f), (h).

Chemical loss and deposition changes become important in remote areas because these areas have the smallest increases in
410   chemical production, but can have the largest changes in loss rate (Fig. S6) and deposition rate. The rate of O_3 loss is correlated
with the change in isoprene concentration, which is typical of a low-NOx region due to reactions between isoprene and O_3
directly (Fig. S7). This leads to increases in the loss rate in most vegetated areas (Fig. S6). Conversely, the deposition rate
decreases, presumably because the increased temperatures and lower relative humidity cause stomatal closure.

415   In high-NOx areas, the increase in O_3 production is greater than the increase in loss leading to net chemical production of O_3.
Evaluation of the sensitivity of O_3 chemical production rate to changes in isoprene emissions and NOx concentration due to
climate change for each model is shown in Fig. 6. NOx decreases in most areas in UKESM1 including high-NOx areas,
whereas GISS and MRI predict increases in NOx (Fig. 6, row 2). The magnitude of the background NOx concentration in
UKESM1 and the change due to climate change is also much larger than the other models. GISS predicts increases of $2x10^{-11}$
420   to $6x10^{-11}$ mol mol^{-1} in high-NOx areas (Fig. 6b), and MRI predicts more uniform increases of $4x10^{-11}$ mol mol^{-1} although
urban areas increase by $8x10^{-11}$ mol mol^{-1} in some cases (Fig. 6c). Despite differences in the magnitude and direction of the
NOx change, the change in O_3 chemical production rate has similar spatial patterns in all models (Fig. 6, row 4). Exceptions
occur in central Africa where GISS predicts a decrease in production rate, and UKESM1 is the only model which does not
predict a large increase in O_3 production in Nigeria. These areas of Africa also exhibit differences in surface O_3 concentration
425   between models, discussed in Sect. 3.3.
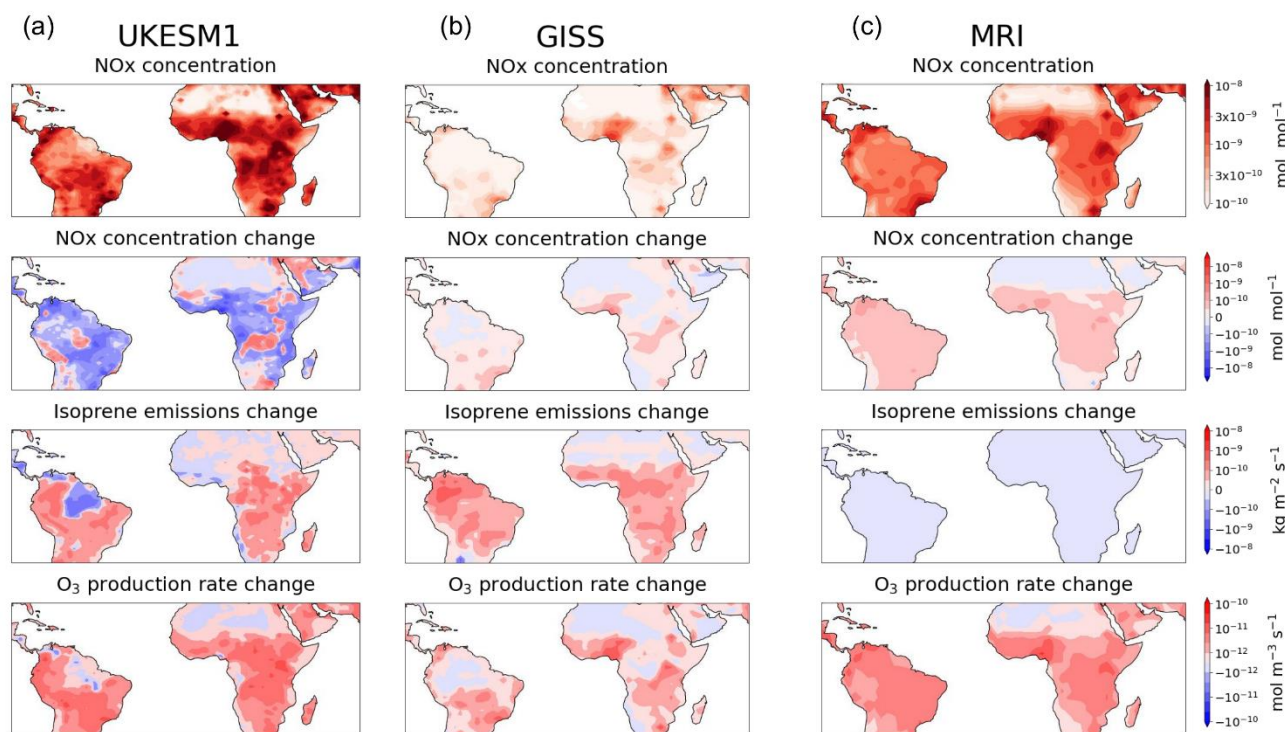
Figure 6: (row 1) Surface NOx concentrations in the absence of climate change and the average change due to climate change in (row 2) NOx concentration, (row 3) isoprene emission rate and (row 4) O3 production rate for the period 2090–2100 for (a) UKESM1, (b) GISS and (c) MRI.

430

On average, isoprene emission rate increases in both GISS and UKESM1, as expected in a warmer climate (MRI does not have interactive isoprene emission) (Fig. 6, row 3). UKESM1 predicts a substantial decrease in isoprene emission rate in the Northern Amazon and fractionally in West Africa (Fig. 6a). Decreases in isoprene emission and stomatal conductance have previously been simulated in the same area due to CO_2 inhibition (Pacifico et al., 2012; Chadwick et al., 2017; Turnock et al.,

435   2020).

The O_3 production rate for GISS appears highly correlated with the change in NOx concentration in Fig. 6b, whereas NOx concentration decreases in many areas where O_3 production increases for UKESM1. Areas in which both NOx and isoprene decrease exhibit decreases in rate of O_3 production, such as the Northern Amazon and Nigeria (Fig. 6a). To determine the

440   strength of the relationship between O_3 production rate and changes in precursors NOx and isoprene, coefficients from a multiple linear regression are presented in Fig. 7. The monthly mean change in isoprene emission rate, NOx concentration and chemical production of O_3 for each grid cell are shown graphically with locations and months of high-NOx (above the 95th percentile) marked with stars. All three climate models produce coefficients between 0.33 and 0.41 for the relationship between changes in NOx concentration and O_3 production rate (Fig. 7). However, the change in isoprene emissions using GISS and

445   UKESM1 is a weaker predictor of O_3 production, even though increases in isoprene emission of over 100 % are predicted. All predictors are considered significant due to the large sample size, with r^2 values of 0.384, 0.732 0.590 for UKESM1, GISS and MRI respectively (S4). The lower r^2 value for UKESM1 indicates that the changes in NOx concentration and isoprene emissions explain less than half of the change in O_3 production rate. Additional analysis shows that the O_3 production rate in UKESM1 is also related to the background NOx concentration (S4).
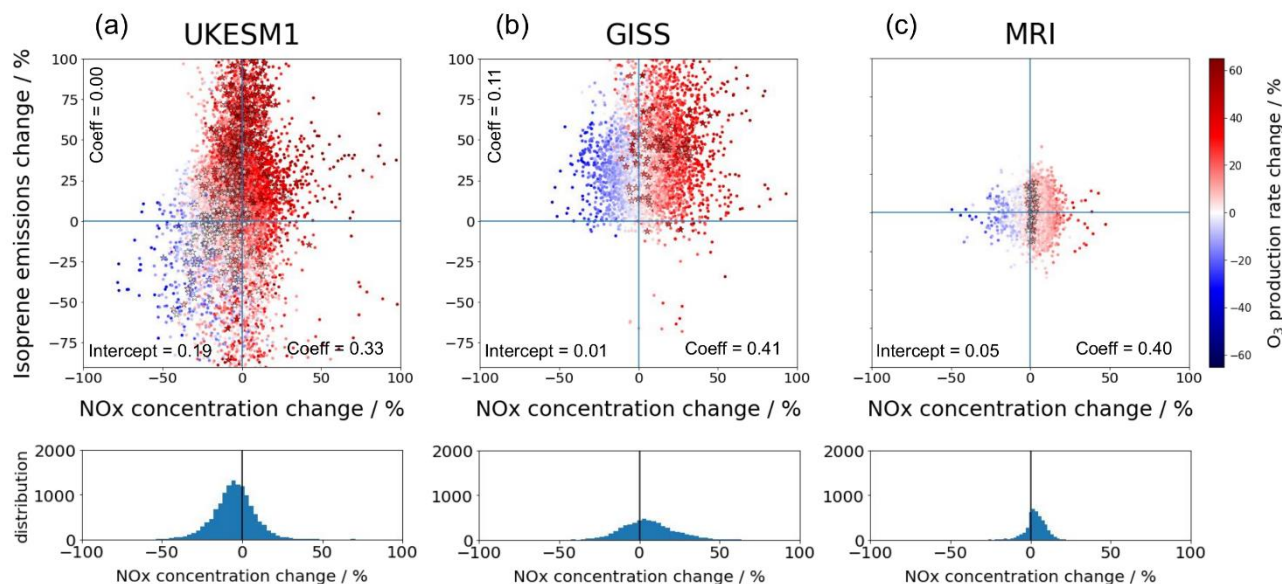
450

Figure 7: Scatter plots of the monthly mean percentage change in surface NOx concentration, isoprene emission rate and O3 production rate for each grid cell and each month for (a) UKESM1, (b) GISS and (c) MRI. Data for MRI has been randomly normally distributed along the y-axis. Grid cells and months where the background NOx concentration is greater than the 95th percentile for the region shown in Fig. 3.1 are marked with stars. The labelled intercept and coefficients refer to the results of a
455 **multiple linear regression ΔO₃ prod (%) ~ ΔNOx (%) + ΔIsoprene (%) using the data plotted. The second row contains the number of data points with each NOx concentration change. The data is divided into 50 bins.**

GISS simulates increases and decreases in NOx concentration of 50 %, compared to the smaller changes predicted by MRI, which fall mostly in the range 0–20 % (Fig. 7c). GISS therefore predicts decreases in production over remote regions (Fig. 6b)
460 and seasons, whereas MRI predicts consistent increases (Fig. 6c). Additionally, high-NOx areas simulated by GISS experience an increase in O3 production regardless of the NOx concentration change (Fig. 7b, stars). In high-NOx areas simulated by UKESM1, the percentage change in NOx concentration is small so there is not enough information to identify individual isoprene and NOx sensitivities, although areas with increased isoprene emission also show increases in O₃ production rate (Fig. 7a, stars).

465

4. Discussion

When compared to in situ observations, the three climate models used in this study overestimate present-day surface O₃ in tropical regions by 14 ppb on average, including 11 ppb over the oceans. This is close to the global bias of 16 ppb calculated by Turnock et al. (2020) which included data from six climate models, including the three in this study. Therefore, the sources

470 of error may not be unique to the tropics. The major sources of variation between model and observations are related to differences in the area sampled and the heights of the stations relative to the lowest model grid cell (Pacifico et al., 2015).

In the tropics, we expect in-canopy deposition and chemical processes to be the most important contributor to the positive bias because these processes create a steep O_3 gradient at the surface, whereas models aim to predict O_3 concentrations at 20+ m

475 from the canopy top where these deposition processes are not included (Stroud et al., 2005; Gordon et al., 2014). Additionally, the volume of the model grid box is many times larger than the area sampled by measurement sites, and also larger than the area of precursor emission sources such as fires. Therefore, the model inputs and predictions represent the average over a region that is not directly comparable with in situ measurements (Sinha et al., 2004). As a further validation, we also provide data from the TES satellite at 825 hPa, which likely records higher O_3 concentrations than the in situ sites since it measures at

480 an altitude away from the canopy sink. Although this is much higher in altitude than the lowest grid box of any of the models, it should capture the above-canopy seasonal cycle at a resolution closer to the model grid resolution.

We find that the modelled surface O_3 bias compared to in situ observations is largest in biomass burning areas, although in South America the models capture the seasonal cycle well (Fig. 1). In situ sites, especially in the DR Congo (Fig. 1e), do not

485 detect the large increases in O_3 predicted by models during biomass burning months although observed O_3 concentrations are also highest during biomass burning season (Adon et al., 2013). It is likely that effective removal within the canopy that is not included in models dampens the observed seasonal cycle. In this region, the trends captured by satellites are closer to the model predictions, which increases confidence that models are correctly identifying O_3 enhancements above the canopy due to fires. However, future studies assessing the risks to human and ecosystem health should be aware of this limitation in current models.

490

The remainder of the study focuses on the change in surface O_3 due to climate change. Although model biases increase uncertainty in the change due to climate change, we quantify the difference between two simulations, which should remove systematic biases, and we note that the models capture seasonal and regional trends that are explained by either in situ measurements or satellite measurements (Fig. 1). This gives confidence in the trends in future O_3 change presented in this

495 study, but we highlight O_3 from biomass burning as an area for further study. The models have different chemistry schemes, land processes and temperature sensitivities which contribute to model variation (Stevenson et al., 2006; Wu et al., 2007; Archibald et al., 2020b). For this reason, we do not attempt to completely diagnose reasons for inter-model variation and instead the aim of this study is to identify robust predictions and areas of uncertainty for the change in O_3 due to climate change.

500

We find that while overall O_3 concentrations over the tropical land areas are reduced under the climate scenario examined here, climate change could lead to an ozone–climate penalty in areas which already have a high background O_3 concentration (above 40 ppb). Models predict that climate change will lead to seasonal mean increases in surface O_3 concentration of up to

505   12 ppb in tropical areas with high-NOx emissions (Fig. 4). The increase in surface O$_3$ in high-NOx areas is robust, with seasonal
mean increases of up to 15 ppb for UKESM1, 18 ppb for GISS and 12 ppb for MRI. These areas are defined by emission
magnitudes above the 95th percentile for the tropics, and often have anthropogenic contributions such as biomass burning or
urban emissions. O$_3$ pollution in forested areas has the potential to reduce forest productivity, decreasing the amount of carbon
removed from the atmosphere and impairing forest resilience (e.g. Sitch et al., 2007; Grulke et al., 2020).

510   The ozone–climate penalty in high-NOx regions is likely to be driven by an increase in chemical production, which is largest
in areas of high-NOx (Figs 5, 6). This is in agreement with results from Doherty et al. (2013) and Archibald et al. (2020b) who
showed that the rate of change of O$_3$ with temperature increases with NOx concentration. Firstly, the reaction happens faster
at higher temperatures and scaling up O$_3$ production in an area where O$_3$ production is already high will often lead to greater
O$_3$ increases than an area with a low O$_3$ precursor concentrations. Secondly the NOx concentration can increase due to
515   increased PAN decomposition at higher temperatures (Doherty et al., 2013), changes in lightning frequency, or changes to
atmospheric chemistry. The modelled O$_3$ increases during burning seasons (dry seasons) are likely compounded by the fact
that these seasons often show the greatest temperature increase due to climate change (Fig. S3). However, we find that lightning
NOx emissions increase in wet seasons suggesting lightning NOx is not a key driver of O$_3$ trends. Some temperature-sensitive
sources of NOx were not included in the simulations such as soil NOx emissions and changes in wildfire frequency. Wildfire
520   feedbacks such as O$_3$ damage to vegetation were also not considered (Pacifico et al., 2015) so future studies could consider
the effect of these sources and feedbacks.

The change in O$_3$ production due to climate change has a high standard deviation in remote regions (Fig. 5d) due to variation
between models in the effect of climate change on NOx concentrations. GISS predicts a decrease in NOx of 2×10^{-11} mol mol^{-1}
525   in remote areas (up to 50 %), which could be related to decreased transport of PAN from source regions and greater loss
through reaction with OH and isoprene. Meanwhile, MRI predicts an increase of 2×10^{-11} to 6×10^{-11} mol mol^{-1} in remote regions.
As NOx concentration has been shown to be a key driver of changes in O$_3$ production due to climate change, further work to
constrain future NOx concentrations is needed to reduce uncertainty in predictions for O$_3$ concentrations.

530   Using a multiple linear regression, we find that changes in NOx concentration have a stronger relationship with changes in O3
production rate than changes in isoprene emissions in GISS and UKESM1 (coefficients of 0.3 – 0.4 compared to ~0.1)
confirming that Africa and South America are NOx-limited on average (Fig. 7). UKESM1 has previously been identified as
being among the least responsive to changes in precursor concentrations out of the CMIP6 models (Turnock et al., 2020), and
we find that linear regression using changes in NOx concentration and isoprene emission explains less than 50 % of the change
535   in O$_3$ production rate. Including background NOx concentration in the linear regression improves the r^2 value and suggests
that, although NOx concentrations in UKESM1 decrease in many areas due to climate change, the rate of O$_3$ production
increases in proportion to the background NOx concentration (Fig. S4). Furthermore, UKESM1 predicts the highest

concentration of background NOx, so high-NOx areas may experience a different chemical regime in which VOCs are also important (e.g. Liu et al., 2013), decreasing linearity in the data.

540

In remote areas, models tend to predict a decrease in surface O_3 over regions strongly affected by ocean air such as North Brazil. This is due to robust decreases in O_3 over the oceans. However, models disagree on the direction of change over inland remote areas (Fig. 4). The increase in chemical production rate is small in these areas compared to high-NOx areas, but the increase in chemical loss is similar in magnitude and these terms act in opposite directions (Fig. 5). The recent study by

545 Zanis et al. (2022) employs 2 additional climate models and also finds climate benefits and uncertainties in surface O_3 concentrations in the same remote regions. We excluded these models from our own study as data for the sensitivity study (NOx concentration and isoprene emission rate) were not available at the time of writing.

The increase in chemical loss is correlated with isoprene concentration, so although it is not limited to low NOx regions it only

550 becomes relevant in magnitude where chemical production is low (Fig. S6). Therefore, the different isoprene schemes used by each model contributes to uncertainty in the loss rate over the continents. In particular, MRI used climatological isoprene resulting in no significant change in the loss rate (Fig. S7) and UKESM1 includes CO_2 inhibition, which decreases the isoprene emission rate and loss rate in in Northern Amazonia (Fig. S6). Overall, this means that GISS has a higher loss rate, which may partly account for the larger decreases in O3 in remote regions using this model (Fig. 8).

555

The global study by Zanis et al. (2022) highlights the different isoprene emission schemes as a reason for model variation however our analysis (Fig. 7) highlights NOx as the most important precursor. The fact that the models contain positive correlations between the change in NOx and O_3 production, and between the change in isoprene and O_3 loss, indicates the tropics exhibit NOx-limited behaviour, although isoprene may be important in high-NOx areas. For example, UKESM1 show

560 increases in O3 production rate as isoprene increases in high-NOx areas (Fig. 7, stars). We also find that isoprene is relevant for the change in loss rate and for indirect effects on O_3 through changes in related atmospheric chemistry (see Isoprene representation in this paper S2).

We finally note that Nigeria experiences substantial increases in O_3 production according to GISS and MRI, whilst a slight

565 decrease is predicted using UKESM1. This is an important geographical area for future research since poor air quality could affect large numbers of people living in West African cities. In this area, the choice of emissions scenario is also important for determining the O_3 response to climate change because NOx emissions in Nigeria increase rapidly in the SSP3-7.0 scenario compared to the present-day due to predicted urbanisation. Therefore, future studies should explore alternative emissions pathways to better inform policy.

5. Conclusion

Using a multimodel mean of data from three Earth system models, we identify that by 2100, there will be an ozone–climate penalty in areas where O_3 due to emissions is already high, such as major cities and biomass burning areas (Fig. 4). This is not due to increased fire emissions, but due to the increasing temperature and associated Earth system changes. It shows that the ozone–climate penalty is greatest in areas already experiencing high O_3, putting forests in these areas at greater risk of O_3 damage and urban populations at increasing threat of health problems. This study adds to findings from the World Health Organisation World Air Quality Report (2021) that air pollution is an increasing issue across the tropics, and that there is a need for greater monitoring of air pollution across Africa and South America.

The Earth system models display NOx-limited behaviour, including that higher NOx concentrations lead to increased O_3 chemical production and therefore increased surface O_3 concentration (Figs 5–7). As the background concentrations of NOx are largely anthropogenic, this suggests that without reduction in emissions, forested areas in urban and fire-prone locations are more at risk from increases in surface O_3 due to climate change than remote forests. As O_3 damage can reduce plant productivity, this has implications for the success of secondary forests and other human-modified forests which are mostly located in agricultural areas, deforestation frontiers and forest edges (Heinrich et al., 2021), and may reduce their carbon sequestration potential (Sitch et al., 2007).

In remote regions, differences in the direction of O_3 concentration change between models creates uncertainty as to whether remote locations are at greater risk of O_3 damage in a warmer climate, although ocean influenced areas display robust climate benefits (Fig. 4). Further work is needed to constrain the climate response of isoprene emissions and the temperature sensitivity of NOx and O_3 chemistry.

Data availability statement

All CMIP6 model data used in the present study can be obtained from https://esgf-node.llnl.gov/search/cmip6/.
All TOAR I data used in the study can be obtained from https://join.fz-juelich.de/services/rest/surfacedata/.
All INDAAF data used in this study can be obtained from http://www.indaaf.obs-mip.fr

Author contributions

FB wrote the paper and led the data analysis with contributions from all authors. SS and GAF contributed to the interpretation of the data. MB contributed to the statistical analysis. IDS, HV, PB, MB and CGL contributed in situ data for model evaluation. SEB and KT contributed in the GISS-E2-1-G simulations; MD and NO contributed in the MRI-ESM2-0 simulations; JK and FMO contributed in the UKESM1-0-LL simulations.

600 **Competing interests**

The authors declare that they have no conflict of interest.

Acknowledgements

FB was funded by the NERC GW4+ DTP (award no. NE/S007504/1) and the Met Office on a CASE studentship. LMM acknowledges funding from the UK Natural Environment Research Council funding (UK Earth System Modelling Project,
605 UKESM, Grant no. NE/N017951/1). SS and LMM were supported by NERC funding (Grant no. NE/R001812/1). MD and NO were supported by the Japan Society for the Promotion of Science KAKENHI (Grant no. JP18H03363, JP18H05292, JP19K12312, JP20K04070 and JP21H03582), the Environment Research and Technology Development Fund (JPMEERF20202003 and JPMEERF20205001) of the Environmental Restoration and Conservation Agency of Japan, the Arctic Challenge for Sustainability II (ArCS II), Program Grant Number JPMXD1420318865, and a grant for the Global
610 Environmental Research Coordination System from the Ministry of the Environment, Japan (MLIT1753). JK was financially supported by NERC through NCAS (Grant no. R8/H12/83/003), and the Met Office CSSP-China programme funded POZsUM project. FMO'C and GAF were supported by the Met Office Hadley Centre Climate Programme funded by BEIS and the EU Horizon 2020 Research Programme CRESCENDO project (Grant no. 641816). Resources supporting the GISS simulations were provided by the NASA High-End Computing (HEC) Program through the NASA Center for
615 Climate Simulation (NCCS) at the Goddard Space Flight Center. GISS authors, SEB and KT acknowledge funding from the NASA Modeling and Analysis program. IV was funded by the Fonds Wetenschappelijk Onderzoek Flanders (FWO; grant no. G018319N). The INDAAF project is funded by the INSU/CNRS/IRD and is part of the ACTRIS-FR Research Infrastructure. The authors are grateful to the field and chemistry analytical technicians who operate the African sites and help to provide reliable data.

620 **References**

Adon, M., Galy-Lacaux, C., Yoboué, V., Delon, C., Lacaux, J. P., Castera, P., Gardrat, E., Pienaar, J., Al Ourabi, H., Laouali, D., Diop, B., Sigha-Nkamdjou, L., Akpo, A., Tathy, J. P., Lavenu, F., and Mougin, E.: Long term measurements of sulfur dioxide, nitrogen dioxide, ammonia, nitric acid and ozone in Africa using passive samplers, Atmos. Chem. Phys., 10, 7467–7487, https://doi.org/10.5194/acp-10-7467-2010, 2010.
625 Adon, M., Galy-Lacaux, C., Delon, C., Yoboue, V., Solmon, F., & Kaptue Tchuente, A. T.: Dry deposition of nitrogen compounds (NO 2, HNO 3, NH 3), sulfur dioxide and O3 in west and central African ecosystems using the inferential method. *Atmospheric Chemistry and Physics*, *13*, 11351-11374. https://doi.org/10.5194/acp-13-11351-2013, 2013

Agathokleous, E., Belz, R. G., Calatayud, V., de Marco, A., Hoshika, Y., Kitao, M., Saitanis, C. J., Sicard, P., Paoletti, E., & Calabrese, E. J.: Predicting the effect of O3 on vegetation via linear non-threshold (LNT), threshold and hormetic dose-response models. *Sci. Total Environ.*, *649*, 61–74. https://doi.org/10.1016/j.scitotenv.2018.08.264, 2019

Archibald, A. T., Jenkin, M. E., & Shallcross, D. E.: An isoprene mechanism intercomparison. *Atmos. Environ.*, *44*, 5356–5364. https://doi.org/10.1016/j.atmosenv.2009.09.016, 2010

Archibald, A. T., O'Connor, F. M., Abraham, N. L., Archer-Nicholls, S., Chipperfield, M. P., Dalvi, M., Folberth, G. A., Dennison, F., Dhomse, S. S., Griffiths, P. T., Hardacre, C., Hewitt, A. J., Hill, R. S., Johnson, C. E., Keeble, J., Köhler, M., Morgenstern, O., Mulcahy, J. P., Ordóñez, C., … Zeng, G.: Description and evaluation of the UKCA stratosphere-troposphere chemistry scheme (StratTrop vn 1.0) implemented in UKESM1. *Geosci. Model Dev.*, *13*, 1223–1266. https://doi.org/10.5194/gmd-13-1223-2020, 2020a

Archibald, A. T., Turnock, S. T., Griffiths, P. T., Cox, T., Derwent, R. G., Knote, C., & Shin, M.: On the changes in surface O3 over the twenty-first century: sensitivity to changes in surface temperature and chemical mechanisms: 21st century changes in surface O3. *Philos. Trans. Royal Soc. A*, *378*. https://doi.org/10.1098/rsta.2019.0329, 2020b

Bela, M. M., Longo, K. M., Freitas, S. R., Moreira, D. S., Beck, V., Wofsy, S. C., Gerbig, C., Wiedemann, K., Andreae, M. O., & Artaxo, P.: O3 production and transport over the Amazon Basin during the dry-to-wet and wet-to-dry transition seasons. *Atmos. Chem. Phys*, *15*, 757–782. https://doi.org/10.5194/acp-15-757-2015, 2015

Bonan, G. B.: Forests and Climate Change: Forcings, Feedbacks, and the Climate Benefits of Forests. *Science*, *320*(5882), 1444–1449. https://doi.org/10.1126/science.1155121, 2008

Bond, D. W., Steiger, S., Zhang, R., Tie, X., & Orville, R. E.: The importance of NO x production by lightning in the tropics. *Atmos. Environ.*, *36*, 1509–1519. https://doi.org/https://doi.org/10.1016/S1352-2310(01)00553-2, 2002

Chadwick, R., Douville, H., & Skinner, C. B.: Timeslice experiments for understanding regional climate projections: applications to the tropical hydrological cycle and European winter circulation. *Clim. Dyn.*, *49*, 3011–3029. https://doi.org/10.1007/s00382-016-3488-6, 2017

Clark, S. K., Ward, D. S., & Mahowald, N. M.: Parameterization-based uncertainty in future lightning flash density. *Geophys. Res. Lett.*, *44*, 2893–2901. https://doi.org/10.1002/2017GL073017, 2017

Clifton, O. E., Fiore, A. M., Massman, W. J., Baublitz, C. B., Coyle, M., Emberson, L., Fares, S., Farmer, D. K., Gentine, P., Gerosa, G., Guenther, A. B., Helmig, D., Lombardozzi, D. L., Munger, J. W., Patton, E. G., Pusede, S. E., Schwede, D. B., Silva, S. J., Sörgel, M., Steiner, A., & Tai, A. P. K.: Dry Deposition of O3 Over Land: Processes, Measurement, and Modeling. *Rev. Geophys.*, *58*. https://doi.org/10.1029/2019RG000670, 2020

Coates, J., Mar, K. A., Ojha, N., & Butler, T. M.: The influence of temperature on O3 production under varying NOx conditions - A modelling study. *Atmos. Chem. Phys*, *16*, 11601–11615. https://doi.org/10.5194/acp-16-11601-2016, 2016

Cox, P. M., Betts, R. A., Collins, M., Harris, P. P., Huntingford, C., & Jones, C. D.: Amazonian forest dieback under climate-carbon cycle projections for the 21st century. *Theor. Appl. Climatol.*, *78*, 137–156. https://doi.org/10.1007/s00704-004-0049-4, 2004

Deushi, M., & Shibata, K.: Impacts of increases in greenhouse gases and O3 recovery on lower stratospheric circulation and the age of air: Chemistry-climate model simulations up to 2100. *J. Geophys. Res*, *116*, 7107. https://doi.org/10.1029/2010JD015024, 2011

665 Doherty, R. M., Wild, O., Shindell, D. T., Zeng, G., MacKenzie, I. A., Collins, W. J., Fiore, A. M., Stevenson, D. S., Dentener, F. J., Schultz, M. G., Hess, P., Derwent, R. G., & Keating, T. J.: Impacts of climate change on surface O3 and intercontinental O3 pollution: A multi-model study. *J. Geophys. Res. Atmos.*, *118*, 3744–3763. https://doi.org/10.1002/jgrd.50266, 2013

Emberson, L.: Effects of O3 on agriculture, forests and grasslands. *Philos. Trans. Royal Soc*, *378*.
670 https://doi.org/10.1098/rsta.2019.0327, 2000

Emberson, L., Kitwiroon, N., Beevers, S., Büker, P., & Cinderby, S.: Scorched earth: How will changes in the strength of the vegetation sink to O3 deposition affect human health and ecosystems? *Atmos. Chem. Phys*, *13*, 6741–6755. https://doi.org/10.5194/acp-13-6741-2013, 2013

Finney, D. L., Doherty, R. M., Wild, O., Stevenson, D. S., Mackenzie, I. A., & Blyth, A. M.: A projected decrease in lightning
675 under climate change. *Nat. Clim. Change., 8*, 210-213. https://doi.org/10.1038/s41558-018-0072-6, 2018

Franz, M., & Zaehle, S.: Competing effects of nitrogen deposition and O3 exposure on Northern hemispheric terrestrial carbon uptake and storage, 1850–2099. *Biogeosci. Discuss.*, 1–42. https://doi.org/10.5194/bg-2020-443, 2020

Fu, T. M., & Tian, H.: Climate Change Penalty to O3 Air Quality: Review of Current Understandings and Knowledge Gaps. *Curr. Poll. Rep.*, *5*, 159–171. https://doi.org/10.1007/s40726-019-00115-6, 2019

680 Fu, Y., & Liao, H.: Biogenic isoprene emissions over China: sensitivity to the CO2 inhibition effect. *Atmos. Ocean Sci. Lett.*, *9*, 277–284. https://doi.org/10.1080/16742834.2016.1187555, 2016

Gordon, M., Vlasenko, A., Staebler, R. M., Stroud, C., Makar, P. A., Liggio, J., Li, S. M., & Brown, S.: Uptake and emission of VOCs near ground level below a mixed forest at Borden, Ontario. *Atmos. Chem. Phys*, *14*, 9087–9097. https://doi.org/10.5194/acp-14-9087-2014, 2014

685 Griffiths, P. T., Murray, L. T., Zeng, G., Shin, Y. M., Abraham, N. L., Archibald, A. T., Deushi, M., Emmons, L. K., Galbally, I. E., Hassler, B., Horowitz, L. W., Keeble, J., Liu, J., Moeini, O., Naik, V., O'Connor, F. M., Oshima, N., Tarasick, D., Tilmes, S., Turnock, S. T., Wild, O., Young, P. J., and Zanis, P.: Tropospheric ozone in CMIP6 simulations, Atmos. Chem. Phys., 21, 4187–4218, https://doi.org/10.5194/acp-21-4187-2021, 2021.

Guenther, A. B., Zimmerman, P. R., Harley, P. C., & Monson, R. K.: Isoprene and Monoterpene Emission Rate Variability'
690 Model Evaluations and Sensitivity Analyses. *J. Geophys. Res. Atmos.*, *98*, 12609–12621. https://doi.org/https://doi.org/10.1029/93JD00527, 1993

Guenther, A., Nicholas Hewitt, ! C, Erickson, D., Fall, R., Geron, C., Graedel, T., Harley, P., Klinger, L., Lerdau, M., Mckay, W. A., Pierce, T., Scholes, B., Steinbrecher, R., Tallamraju, R., Taylor, J., & Zimmerman, P.: A global model of natural volatile organic compound emissions. *J. Geophys. Res. Atmos.*, *100*, 8873–8892.
695 https://doi.org/https://doi.org/10.1029/94JD02950, 1995

Hantson, S., Knorr, W., Schurgers, G., Pugh, T. A. M., & Arneth, A.: Global isoprene and monoterpene emissions under changing climate, vegetation, CO2 and land use. *Atmos. Environ.*, *155*, 35–45. https://doi.org/10.1016/j.atmosenv.2017.02.010, 2017

Heinrich, V. H. A., Dalagnol, R., Cassol, H. L. G., Rosan, T. M., Torres De Almeida, C., Silva Junior, C. H. L., Campanharo, W. A., House, J. I., Sitch, S., Hales, T. C., Adami, M., Anderson, L. O., Luiz, &, & Aragão, E. O. C.: Large carbon sink potential of secondary forests in the Brazilian Amazon to mitigate climate change. *Nat. Commun.*, *12*, 1–11. https://doi.org/10.1038/s41467-021-22050-1, 2021

Jacob, D. J., & Winner, D. A. (2009). Effect of climate change on air quality. *Atmos. Environ.*, *43*, 51–63. https://doi.org/10.1016/j.atmosenv.2008.09.051

Jacobs, C. M. J.: Direct impact of atmospheric CO2 enrichment on regional transpiration. *Wageningen University and Research*. https://doi.org/10.5194/gmd-12-2875-2019, 1994

Kawai, H., Yukimoto, S., Koshiro, T., Oshima, N., Tanaka, T., Yoshimura, H., and Nagasawa, R.: Significant improvement of cloud representation in the global climate model MRI-ESM2, Geosci. Model Dev., 12, 2875–2897, https://doi.org/10.5194/gmd-12-2875-2019, 2019.

Kelley, M., Schmidt, G. A., Nazarenko, L. S., Bauer, S. E., Ruedy, R., Russell, G. L., Ackerman, A. S., Aleinov, I., Bauer, M., Bleck, R., Canuto, V., Cesana, G., Cheng, Y., Clune, T. L., Cook, B. I., Cruz, C. A., Del Genio, A. D., Elsaesser, G. S., Faluvegi, G., Kiang, N. Y., Kim, D., Lacis, A. A., Leboissetier, A., LeGrande, A. N., Lo, K. K., Marshall, J., Matthews, E. E., McDermid, S., Mezuman, K., Miller, R. L., Murray, L. T., Oinas, V., Orbe, C., Pérez García-Pando, C., Perlwitz, J. P., Puma, M. J., Rind, D., Romanou, A., Shindell, D. T., Sun, S., Tausnev, N., Tsigaridis, K., Tselioudis, G., Weng, E., Wu, J., and Yao, M.-S.: GISS-E2.1: Configurations and Climatology, J. Adv. Model. Earth Sy., 12, e2019MS002025, https://doi.org/10.1029/2019MS002025, 2020.

Kuhn, U., Ganzeveld, L., Thielmann, A., Dindorf, T., Schebeske, G., Welling, M., Sciare, J., Roberts, G., Meixner, F. X., Kesselmeier, J., Lelieveld, J., Kolle, O., Ciccioli, P., Lloyd, J., Trentmann, J., Artaxo, P., & Andreae, M. O.: Impact of Manaus City on the Amazon Green Ocean atmosphere: O3 production, precursor sensitivity and aerosol load. *Atmos. Chem. Phys*, *10*, 9251–9282. https://doi.org/10.5194/acp-10-9251-2010, 2010

Leuning, R.: A critical appraisal of a combined stomatal-photosynthesis model for C3 plants. *Plant, Cell Environ.*, *18*, 339–355. https://doi.org/https://doi.org/10.1111/j.1365-3040.1995.tb00370.x, 1995

Lewis, S. L.: Tropical forests and the changing earth system. *Philos. Trans. Royal Soc. B*, *361*, 195–210. https://doi.org/10.1098/rstb.2005.1711, 2006

Lin, M., Horowitz, L. W., Xie, Y., Paulot, F., Malyshev, S., Shevliakova, E., Finco, A., Gerosa, G., Kubistin, D., & Pilegaard, K.: Vegetation feedbacks during drought exacerbate O3 air pollution extremes in Europe. *Nat. Clim. Change*, *10*, 444–451. https://doi.org/10.1038/s41558-020-0743-y, 2020a

Liu, W., Hegglin, M. I., Checa-Garcia, R., Li, S., Gillett, N. P., Lyu, K., Zhang,X., & Swart, N. C.: Stratospheric ozone depletion and tropospheric ozone increases drive Southern Ocean interior warming. *Nat. Clim. Change*, *12,* 365–372. https://doi.org/10.1038/s41558-022-01320-w, 2022

Liu, Y., Brito, J., Dorris, M. R., Rivera-Rios, J. C., Seco, R., Bates, K. H., Artaxo, P., Duvoisin, S., Keutsch, F. N., Kim, S., Goldstein, A. H., Guenther, A. B., Manzi, A. O., Souza, R. A. F., Springston, S. R., Watson, T. B., McKinney, K. A., & Martin, S. T.: Isoprene photochemistry over the Amazon rainforest. *Proc. Natl. Acad. Sci U.S.A*, *113*, 6125–6130. https://doi.org/10.1073/pnas.1524136113, 2016

Liu, Z., Doherty, R. M., Wild, O., Hollaway, M., & O'Connor, F. M: Contrasting chemical environments in summertime for atmospheric O3 across major Chinese industrial regions: the effectiveness of emission control strategies. *Atmospheric Chemistry and Physics*, *21*, 10689–10706. https://doi.org/10.5194/acp-21-10689-2021, 2021

Malhi, Y., Aragã O A, L. E. O. C., Galbraith, D., Huntingford, C., Fisher, R., Zelazowski, P., Sitch, S., Mcsweeney, C., & Meir, P.: Exploring the likelihood and mechanism of a climate-change-induced dieback of the Amazon rainforest. *Proc. Natl. Acad. Sci*, *106*, 20610-20615. https://doi.org/10.1073/pnas.0804619106, 2009

Meinshausen, M., Nicholls, Z. R. J., Lewis, J., Gidden, M. J., Vogel, E., Freund, M., Beyerle, U., Gessner, C., Nauels, A., Bauer, N., Canadell, J. G., Daniel, J. S., John, A., Krummel, P. B., Luderer, G., Meinshausen, N., Montzka, S. A., Rayner, P. J., Reimann, S., Smith, S. J., van den Berg, M., Velders, G. J. M., Vollmer, M. K., and Wang, R. H. J.: The shared socio-economic pathway (SSP) greenhouse gas concentrations and their extensions to 2500, Geosci. Model Dev., 13, 3571–3605, https://doi.org/10.5194/gmd-13-3571-2020, 2020.

Morfopoulos, C., Müller, J. F., Stavrakou, T., Bauwens, M., de Smedt, I., Friedlingstein, P., Prentice, I. C., & Regnier, P.: Vegetation responses to climate extremes recorded by remotely sensed atmospheric formaldehyde. *Glob. Change. Biol.*. *28*, 1809–1822. https://doi.org/10.1111/gcb.15880, 2021

Mulcahy, J. P., Jones, C., Sellar, A., Johnson, B., Boutle, I. A., Jones, A., Andrews, T., Rumbold, S. T., Mollard, J., Bellouin, N., Johnson, C. E., Williams, K. D., Grosvenor, D. P., & Mccoy, D. T. Improved Aerosol Processes and Effective Radiative Forcing in HadGEM3 and UKESM1. *J. Adv. Model. Earth Syst.*, *10*, 2786–2805. https://doi.org/10.1029/2018MS001464, 2018

Mulcahy, J. P., Johnson, C., Jones, C. G., Povey, A. C., Scott, C. E., Sellar, A., Turnock, S. T., Woodhouse, M. T., Abraham, N. L., Andrews, M. B., Bellouin, N., Browse, J., Carslaw, K. S., Dalvi, M., Folberth, G. A., Glover, M., Grosvenor, D. P., Hardacre, C., Hill, R., Johnson, B., Jones, A., Kipling, Z., Mann, G., Mollard, J., O'Connor, F. M., Palmiéri, J., Reddington, C., Rumbold, S. T., Richardson, M., Schutgens, N. A. J., Stier, P., Stringer, M., Tang, Y., Walton, J., Woodward, S., and Yool, A.: Description and evaluation of aerosol in UKESM1 and HadGEM3-GC3.1 CMIP6 historical simulations, Geosci. Model Dev., 13, 6383–6423, https://doi.org/10.5194/gmd-13-6383-2020, 2020.

Murray, L. T.: Lightning NO x and Impacts on Air Quality. *Curr. Poll. Rep.*, *2*, 115–133. https://doi.org/10.1007/s40726-016-0031-7, 2016

Niinemets U., Tenhunen J.D., Harley P.C., & Steinbrecher R.: A model of isoprene emission based on energetic requirements for isoprene synthesis and leaf photosynthetic properties for Liquidambar and Quercus. *Plant, Cell Environ.*, *22*, 1319–1335. https://doi.org/https://doi.org/10.1046/j.1365-3040.1999.00505.x, 1999

Oshima, N., Yukimoto, S., Deushi, M., Koshiro, T., Kawai, H., Tanaka, T. Y., & Yoshida, K.: Global and Arctic effective radiative forcing of anthropogenic gases and aerosols in MRI-ESM2. 0. *Progress in Earth and Planetary Science*, *7*, 1-21. https://doi.org/10.1186/s40645-020-00348-w, 2020

Ossohou, M., Galy-Lacaux, C., Yoboué, V., Hickman, J. E., Gardrat, E., Adon, M., Darras, S., Laouali, D., Akpo, A., Ouafo, M., Diop, B., & Opepa, C.: Trends and seasonal variability of atmospheric NO2 and HNO3 concentrations across three major African biomes inferred from long-term series of ground-based and satellite measurements. *Atmos. Environ.*, *207*, 148-166. https://doi.org/10.1016/j.atmosenv.2019.03.027, 2019

Oswald, E. M., Dupigny-Giroux, L. A., Leibensperger, E. M., Poirot, R., & Merrell, J.: Climate controls on air quality in the Northeastern U.S.: An examination of summertime O3 statistics during 1993-2012. *Atmos. Environ.*, *112*, 278–288. https://doi.org/10.1016/j.atmosenv.2015.04.019, 2015

Pacifico, F., Harrison, S. P., Jones, C. D., Arneth, A., Sitch, S., Weedon, G. P., Barkley, M. P., Palmer, P. I., Serça, D., Potosnak, M., Fu, T. M., Goldstein, A., Bai, J., & Schurgers, G.: Evaluation of a photosynthesis-based biogenic isoprene emission scheme in JULES and simulation of isoprene emissions under present-day climate conditions. *Atmos. Chem. Phys*, *11*, 4371–4389. https://doi.org/10.5194/acp-11-4371-2011, 2011

Pacifico, F., Folberth, G. A., Jones, C. D., Harrison, S. P., & Collins, W. J: Sensitivity of biogenic isoprene emissions to past, present, and future environmental conditions and implications for atmospheric chemistry. *J. Geophys. Res. Atmos.*, *117*. https://doi.org/10.1029/2012JD018276, 2012

Pacifico, F., Folberth, G. A., Sitch, S., Haywood, J. M., Rizzo, L. v., Malavelle, F. F., & Artaxo, P.: Biomass burning related O3 damage on vegetation over the Amazon forest: A model sensitivity study. *Atmos. Chem. Phys*, *15*, 2791–2804. https://doi.org/10.5194/acp-15-2791-2015, 2015

Pascoe, C., Lawrence, B. N., Guilyardi, E., Juckes, M., & Taylor, K. E.: Designing and Documenting Experiments in CMIP6. *Geosci. Model Dev. Discuss.*, *10*, 1–27. https://doi.org/10.5194/gmd-2019-98, 2019

Paulot, F., Henze, D. K., & Wennberg, P. O.: Impact of the isoprene photochemical cascade on tropical O3. *Atmos. Chem. Phys*, *12*, 1307–1325. https://doi.org/10.5194/acp-12-1307-2012, 2012

Price, C., & Rind, D.: A Simple Lightning Parameterization for Calculating Global Lightning Distributions. *J. Geophys. Res.*, *97*, 9919–9933. https://doi.org/https://doi.org/10.1029/92JD00719, 2018

Prosperi, P., Bloise, M., Tubiello, F. N., Conchedda, G., Rossi, S., Boschetti, L., Salvatore, M., & Bernoux, M: New estimates of greenhouse gas emissions from biomass burning and peat fires using MODIS Collection 6 burned areas. *Clim. Change*, *161*, 415–432. https://doi.org/10.1007/s10584-020-02654-0, 2020

Pugh, T. A. M., Mackenzie, A. R., Hewitt, C. N., Langford, B., Edwards, P. M., Furneaux, K. L., Heard, D. E., Hopkins, J. R., Jones, C. E., Karunaharan, A., Lee, J., Mills, G., Misztal, P., Moller, S., Monks, P. S., & Whalley, L. K.: Simulating

795   atmospheric composition over a South-East Asian tropical rainforest: performance of a chemistry box model. *Atmos. Chem. Phys*, *10*, 279–298. https://doi.org/https://doi.org/10.5194/acp-10-279-2010, 2010

Rao, S., Klimont, Z., Smith, S. J., Van Dingenen, R., Dentener, F., Bouwman, L., Riahi, K., Amann, M., Bodirsky, B. L., van Vuuren, D. P., Reis, L. A., Calvin, K., Drouet, L., Fricko, O., Fujimori, S., Gernaat, D., Havlik, P., Harmsen, M., Hasegawa, T., Heyes, C., Hilaire, J., Luderer, G., Masui, T., Stehfest, E., Strefler, J., van der Sluis, S., and Tavoni, M.:

800   Future air pollution in the Shared Socio-economic Pathways, Global Environ. Chang., 42, 346–358, https://doi.org/10.1016/j.gloenvcha.2016.05.012, 2017.

Riahi, K., van Vuuren, D. P., Kriegler, E., Edmonds, J., O'Neill, B. C., Fujimori, S., Bauer, N., Calvin, K., Dellink, R., Fricko, O., Lutz, W., Popp, A., Cuaresma, J. C., K.-C, S., Leimbach, M., Jiang, L., Kram, T., Rao, S., Emmerling, J., Ebi, K., Hasegawa, T., Havlik, P., Humpenöder, F., Silva, L. A. D., Smith, S., Stehfest, E., Bosetti, V., Eom, J., Gernaat, D.,

805   Masui, T., Rogelj, J., Strefler, J., Drouet, L., Krey, V., Luderer, G., Harmsen, M., Takahashi, K., Baumstark, L., Doelman, J. C., Kainuma, M., Klimont, Z., Marangoni, G., Lotze-Campen, H., Obersteiner, M., Tabeau, A., and Tavoni, M.: The Shared Socioeconomic Pathways and their energy, land use, and greenhouse gas emissions implications: An overview, Global Environ. Change, 42, 153–168, https://doi.org/10.1016/j.gloenvcha.2016.05.009, 2017.

Romer, P. S., Duffey, K. C., Wooldridge, P. J., Edgerton, E., Baumann, K., Feiner, P. A., Miller, D. O., Brune, W. H., Koss,

810   A. R., de Gouw, J. A., Misztal, P. K., Goldstein, A. H., & Cohen, R. C.: Effects of temperature-dependent NOx emissions on continental O3 production. *Atmos. Chem. Phys*, *18*, 2601–2614. https://doi.org/10.5194/acp-18-2601-2018, 2018

Sadiq, M., Tai, A. P. K., Lombardozzi, D., & Martin, M. V.: Effects of O3-vegetation coupling on surface O3 air quality via biogeochemical and meteorological feedbacks. *Atmos. Chem. Phys*, *17*, 3055–3066. https://doi.org/10.5194/acp-17-3055-2017, 2017

815   Sanderson, M. G., Jones, C. D., Collins, W. J., Johnson, C. E., & Derwent, R. G.: Effect of climate change on isoprene emissions and surface O3 levels. *Geophys. Res. Lett.*, *30*. https://doi.org/10.1029/2003GL017642, 2003

Schröder. TOAR Data Infrastructure. *https://doi.org/10.34730/4d9a287dec0b42f1aa6d244de8f19eb3*, 2021

Schultz, M. G., Jacob, D. J., Wang, Y., Logan, J. A., Atlas, E. L., Blake, D. R., Blake, N. J., Bradshaw, J. D., Browell, E. v, Fenn, M. A., Flocke, F., Gregory, G. L., Heikes, B. G., Sachse, G. W., Sandholm, S. T., Shetter, R. E., Singh, H. B., &

820   Talbot, R. W.: On the origin of tropospheric O3 and NOx over the tropical South Pacific. *J. Geophys. Res.*, *104*, 5829–5843. https://doi.org/10.1029/98JD02309, 1999

Schultz, MG, Schröder, S, Lyapina, O, Cooper, OR, Galbally, I, Petropavlovskikh, I, von Schneidemesser, E, Tanimoto, H, Elshorbany, Y, Naja, M, Seguel, RJ, Dauert, U, Eckhardt, P, Feigenspan, S, Fiebig, M, Hjellbrekke, A-G, Hong, Y-D, Kjeld, PC, Koide, H, Lear, G, Tarasick, D, Ueno, M, Wallasch, M, Baumgardner, D, Chuang, M-T, Gillett, R, Lee, M,

825   Molloy, S, Moolla, R, Wang, T, Sharps, K, Adame, JA, Ancellet, G, Apadula, F, Artaxo, P, Barlasina, ME, Bogucka, M, Bonasoni, P, Chang, L, Colomb, A, Cuevas-Agulló, E, Cupeiro, M, Degorska, A, Ding, A, Fröhlich, M, Frolova, M, Gadhavi, H, Gheusi, F, Gilge, S, Gonzalez, MY, Gros, V, Hamad, SH, Helmig, D, Henriques, D, Hermansen, O, Holla, R, Hueber, J, Im, U, Jaffe, DA, Komala, N, Kubistin, D, Lam, K-S, Laurila, T, Lee, H, Levy, I, Mazzoleni, C, Mazzoleni,

830   LR, McClure-Begley, A, Mohamad, M, Murovec, M, Navarro-Comas, M, Nicodim, F, Parrish, D, Read, KA, Reid, N, Ries, L, Saxena, P, Schwab, JJ, Scorgie, Y, Senik, I, Simmonds, P, Sinha, V, Skorokhod, AI, Spain, G, Spangl, W, Spoor, R, Springston, SR, Steer, K, Steinbacher, M, Suharguniyawan, E, Torre, P, Trickl, T, Weili, L, Weller, R, Xiaobin, X, Xue, L and Zhiqiang, M: Tropospheric O3 Assessment Report: Database and metrics data of global surface O3 observations. *Elm Sci Anth*, *58*, https://doi.org/10.1525/elementa.244, 2017

Sellar, A. A., Jones, C. G., Mulcahy, J. P., Tang, Y., Yool, A., Wiltshire, A., O'Connor, F. M., Stringer, M., Hill, R., Palmieri,
835   J., Woodward, S., Mora, L. d., Kuhlbrodt, T., Rumbold, S. T., Kelley, D. I., Ellis, R., Johnson, C. E., Walton, J., Abraham, N. L., Andrews, M. B., Andrews, T., Archibald, A. T., Berthou, S., Burke, E., Blockley, E., Carslaw, K., Dalvi, M., Edwards, J., Folberth, G. A., Gedney, N., Griffiths, P. T., Harper, A. B., Hendry, M. A., Hewitt, A. J., Johnson, B., Jones, A., Jones, C. D., Keeble, J., Liddicoat, S., Morgenstern, O., Parker, R. J., Predoi, V., Robertson, E., Siahaan, A., Smith, R. S., Swaminathan, R., Woodhouse, M. T., Zeng, G., and Zerroukat, M.: UKESM1: Description
840   and Evaluation of the U.K. Earth System Model, J. Adv. Modeling Earth Sy., 11, 4513–4558, https://doi.org/10.1029/2019MS001739, 2019.

Shindell, D. T., Faluvegi, G., Unger, N., Aguilar, E., Schmidt, G. A., Koch, D. M., Bauer, S. E., & Miller, R. L.: Simulations of preindustrial, present-day, and 2100 conditions in the NASA GISS composition and climate model G-PUCCINI. *Atmos. Chem. Phys*, *6*, 4427–4459. https://doi.org/10.5194/acp-6-4427-2006, 2006

845   Shindell, D. T., Pechony, O., Voulgarakis, A., Faluvegi, G., Nazarenko, L., Lamarque, J. F., Bowman, K., Milly, G., Kovari, B., Ruedy, R., & Schmidt, G. A.: Interactive O3 and methane chemistry in GISS-E2 historical and future climate simulations. *Atmos. Chem. Phys*, *13*, 2653–2689. https://doi.org/10.5194/acp-13-2653-2013, 2013

Shi, Y., Zang, S., Matsunaga, T., & Yamaguchi, Y.: A multi-year and high-resolution inventory of biomass burning emissions in tropical continents from 2001–2017 based on satellite observations. *Journal of Cleaner Production*, *270*, 122511.
850   https://doi.org/10.1016/j.jclepro.2020.122511, 2020

Silva, S. J., & Heald, C. L.: Investigating Dry Deposition of O3 to Vegetation. *J. Geophys. Res. Atmos.*, *123*, 559–573. https://doi.org/10.1002/2017JD027278, 2018

Sinha, P., Jaeglé, L., Hobbs, P. v, & Liang, Q.: Transport of biomass burning emissions from southern Africa. *J. Geophys. Res*, *109*, 20204. https://doi.org/10.1029/2004JD005044, 2004

855   Sitch, S., Cox, P. M., Collins, W. J., & Huntingford, C.: Indirect radiative forcing of climate change through O3 effects on the land-carbon sink. *Nature*, *448*, 791–794. https://doi.org/10.1038/nature06059, 2007

Squire, O. J., Archibald, A. T., Abraham, N. L., Beerling, D. J., Hewitt, C. N., Lathière, J., Pike, R. C., Telford, P. J., & Pyle, J. A.: Influence of future climate and cropland expansion on isoprene emissions and tropospheric O3. *Atmos. Chem. Phys*, *14*, 1011–1024. https://doi.org/10.5194/acp-14-1011-2014, 2014

860   Squire, O. J., Archibald, A. T., Griffiths, P. T., Jenkin, M. E., Smith, D., & Pyle, J. A.: Influence of isoprene chemical mechanism on modelled changes in tropospheric O3 due to climate and land use over the 21st century. *Atmos. Chem. Phys*, *15*, 5123–5143. https://doi.org/10.5194/acp-15-5123-2015, 2015

Stevenson, D. S., Dentener, F. J., Schultz, M. G., Ellingsen, K., van Noije, T. P. C., Wild, O., Zeng, G., Amann, M., Atherton, C. S., Bell, N., Bergmann, D. J., Bey, I., Butler, T., Cofala, J., Collins, W. J., Derwent, R. G., Doherty, R. M., Drevet,

865   J., Eskes, H. J., Fiore, A. M., Gauss, M., Hauglustaine, D. A., Horowitz, L. W., Isaksen, I. S. A., Krol, M. C., Lamarque, J.-F., Lawrence, M. G., Montanaro, V., Muller, J. F., Pitari, G., Prather, M. J., Pyle, J. A., Rast, S., Rodriguez, J. M., Sanderson, M. G., Savage, N. H., Shindell, D. T., Strahan, S. E., Sudo, K., and Szopa, S.: Multimodel ensemble simulations of present-day and near-future tropospheric ozone, J. Geophys. Res., 111, D08301, https://doi.org/10.1029/2005JD006338, 2006.

870   Stroud, C., Makar, P., Karl, T., Guenther, A., Geron, C., Turnipseed, A., Nemitz, E., Baker, B., Potosnak, M., Fuentes, J. D., Stroud, C. :, Makar, P., Karl, T., Guenther, A., Geron, C., Turnipseed, A., Nemitz, E., Baker, B., Potosnak, M., & Fuentes, J. D.: Role of canopy-scale photochemistry in modifying biogenic-atmosphere exchange of reactive terpene species: Results from the CELTIC field study. *J. Geophys. Res*, *110*, 17303. https://doi.org/10.1029/2005JD005775, 2005

875   Tsigaridis, K., & Kanakidou, M.: The present and future of secondary organic aerosol direct forcing on climate. *Current Climate Change Reports*, *4*, 84-98. https://doi.org/10.1007/s40641-018-0092-3, 2018

Turnock, S. T., Allen, R. J., Andrews, M., Bauer, S. E., Deushi, M., Emmons, L., Good, P., Horowitz, L., John, J. G., Michou, M., Nabat, P., Naik, V., Neubauer, D., O'Connor, F. M., Olivié, D., Oshima, N., Schulz, M., Sellar, A., Shim, S., Takemura, T., Tilmes, S., Tsigaridis, K., Wu, T., and Zhang, J.: Historical and future changes in air pollutants from

880   CMIP6 models, Atmos. Chem. Phys., 20, 14547–14579, https://doi.org/10.5194/acp-20-14547-2020, 2020.

Turnock, S. T., Wild, O., Sellar, A., & O'Connor, F. M: 300 years of tropospheric O3 changes using CMIP6 scenarios with a parameterised approach. *Atmos. Environ.*, *213*, 686–698. https://doi.org/10.1016/j.atmosenv.2019.07.001, 2019

Unger, N., Harper, K., Zheng, Y., Kiang, N. Y., Aleinov, I., Arneth, A., Schurgers, G., Amelynck, C., Goldstein, A., Guenther, A., Heinesch, B., Hewitt, C. N., Karl, T., Laffineur, Q., Langford, B., A. McKinney, K., Misztal, P., Potosnak, M., Rinne,

885   J., Pressley, S., Schoon, N., and Serça, D.: Photosynthesis-dependent isoprene emission from leaf to planet in a global carbon-chemistry-climate model, Atmos. Chem. Phys., 13, 10243–10269, https://doi.org/10.5194/acp-13-10243-2013, 2013.

Weber, J., Archer-Nicholls, S., Abraham, N. L., Shin, Y. M., Bannan, T. J., Percival, C. J., Bacak, A., Artaxo, P., Jenkin, M., Khan, M. A. H., Shallcross, D. E., Schwantes, R. H., Williams, J., & Archibald, A. T.: Improvements to the

890   representation of BVOC chemistry-climate interactions in UKCA (v11.5) with the CRI-Strat 2 mechanism: Incorporation and evaluation. *Geosci. Model Dev.*, *14*, 5239–5268. https://doi.org/10.5194/gmd-14-5239-2021, 2021

Wedow, J. M., Ainsworth, E. A., & Li, S.: Plant biochemistry influences tropospheric O3 formation, destruction, deposition, and response. *Trends Biochem. Sci*, *46*, 992–1002. https://doi.org/10.1016/j.tibs.2021.06.007, 2021

Wild, O., Voulgarakis, A., O'Connor, F., Lamarque, J. F., Ryan, E. M., & Lee, L.: Global sensitivity analysis of chemistry-

895   climate model budgets of tropospheric O3 and OH: Exploring model diversity. *Atmos. Chem. Phys*, *20*, 4047–4058. https://doi.org/10.5194/acp-20-4047-2020, 2020

Williams, K. D., Copsey, D., Blockley, E. W., Bodas-Salcedo, A., Calvert, D., Comer, R., Davis, P., Graham, T., Hewitt, H. T., Hill, R., Hyder, P., Ineson, S., Johns, T. C., Keen, A. B., Lee, R. W., Megann, A., Milton, S. F., Rae, J. G. L., Roberts, M. J., Scaife, A. A., Schiemann, R., Storkey, D., Thorpe, L., Watterson, I. G., Walters, D. N., West, A., Wood, R. A., Woollings, T., and Xavier, P. K.: The Met Office Global Coupled Model 3.0 and 3.1 (GC3.0 and GC3.1) Configurations, J. Adv. Model. Earth Sy., 10, 357–380, https://doi.org/10.1002/2017MS001115, 2018.

Wiltshire, A. J., Duran Rojas, M. C., Edwards, J. M., Gedney, N., Harper, A. B., Hartley, A. J., Hendry, M. A., Robertson, E., and Smout-Day, K.: JULES-GL7: the Global Land configuration of the Joint UK Land Environment Simulator version 7.0 and 7.2, Geosci. Model Dev., 13, 483–505, https://doi.org/10.5194/gmd-13-483-2020, 2020.

Wiltshire, A. J., Burke, E. J., Chadburn, S. E., Jones, C. D., Cox, P. M., Davies-Barnard, T., Friedlingstein, P., Harper, A. B., Liddicoat, S., Sitch, S., and Zaehle, S.: JULES-CN: a coupled terrestrial carbon–nitrogen scheme (JULES vn5.1), Geosci. Model Dev., 14, 2161–2186, https://doi.org/10.5194/gmd-14-2161-2021, 2021.

World Health Organisation: World Air Quality Report, available at: https://www.iqair.com/world-air-quality-report, 2021

Wu, S., Mickley, L. J., Jacob, D. J., Logan, J. A., Yantosca, R. M., & Rind, D: Why are there large differences between models in global budgets of tropospheric O3? *J. Geophys. Res. Atmos.*, *112*. https://doi.org/10.1029/2006JD007801, 2007

Yue, X., & Unger, N.: Fire air pollution reduces global terrestrial productivity. *Nat. Commun.*, *9*, 1–9. https://doi.org/10.1038/s41467-018-07921-4, 2018

Yukimoto, S., Kawai, H., Koshiro, T., Oshima, N., Yoshida, K., Urakawa, S., Tsujino, H., Deushi, M., Tanaka, T., Hosaka, M., Yabu, S., Yoshimura, H., Shindo, E., Mizuta, R., Obata, A., Adachi, Y., & Ishii, M.: The meteorological research institute Earth system model version 2.0, MRI-ESM2.0: Description and basic evaluation of the physical component. *J. Meteorol. Soc. .Japan*, *97*, 931–965. https://doi.org/10.2151/jmsj.2019-051, 2019

Zanis, P., Turnock, S., Naik, V., Szopa, S., K Georgoulias, A., Bauer, S. E., Deushi, M., Horowitz, L. W., Keeble, J., le Sager, P., O, F. M., Oshima, N., Tsigaridis, K., & van Noije, T.: *Climate change penalty and benefit on surface O3: A global perspective based on CMIP6 earth system models*, [preprint] https://doi.org/10.1088/1748-9326/ac4a34 , 2022

Zeng, G., Pyle, J. A., & Young, P. J.: Impact of climate change on tropospheric O3 and its global budgets. *Atmos. Chem. Phys*, *8*, 369–387. https://doi.org/10.5194/acp-8-369-2008, 2008

Ziemke, J. R., Chandra, S., Duncan, B. N., Schoeberl, M. R., Torres, O., Damon, M. R., & Bhartia, P. K.: Recent biomass burning in the tropics and related changes in tropospheric O3. *Geophys. Res. Lett.*, *36*. https://doi.org/10.1029/2009GL039303, 2009